Accurate Quantitation of Phospholamban Expression and Phosphorylation in Biological Samples

A Dissertation
SUBMITTED TO THE FACULTY OF
UNIVERSITY OF MINNESOTA
BY

Naa-Adjeley D. Ablorh

IN PARTIAL FULFILLMENT OF THE REQUIREMENTS
FOR THE DEGREE OF
DOCTOR OF PHILOSOPHY

David D. Thomas

June, 2013

Acknowledgements

This work was supported in part by grants to DDT (NIH GM27906, NIH P30 AR057220), NAA (NIH F31 HL090074), SJG (American Heart Association), and JH (HealthPartners Research Foundation 06-032). This project used the excellent facilities of the Minnesota Supercomputing Institute and the Biophysical Spectroscopy Facility. We thank Christine Karim for providing synthetic PLB standards and Octavian Cornea for assistance with manuscript preparation.

Premium thanks to David Dale Thomas, who gave me the opportunity to join his lab, and guided me to successful publications, grants, and awards. His direct approach to improving my performance left no ambiguity about his faith in my potential as a scientist. He also lightened the load of PhD work by celebrating at parties in the lab and at his house. Some of them were in celebration of specific accomplishments, and others for a general appreciation for camaraderie in the lab and in life. For the parties at the Thomas's house, I also thank Jennifer Jewell Thomas for planning and hosting great parties.

I thank my mentors: Christine Karim, who taught me how to plan experiments, showed me how to manage my time, and encouraged me to collaborate with others; Vincent Barnett, a former member of the Dave Thomas lab, who helped me to absorb the culture of the lab; Peter Pesheck, who introduced me to industry, taught me about data presentation, improved my writing greatly by introducing me to Strunk & White, and transferred (by osmosis) his fervor for solving scientific problems; Jenni Swenson, who introduced me to academia; and Noro Andriamanalina, who gave me encouragement and career advice. I would also like to thank Barb Blacklock, who encouraged me to be proactive in seeking the equipment and assistance that would allow me to succeed.

I thank my Collaborators: Florentin Nitu, who taught me several skills in the laboratory, including how to perform western blots, and gave me advice on my experimental planning during my weekly meetings with Dave. I thank Joel Holger and Kristen Engebretsen, for making my first publication possible. I thank Junior scientists Tyler Miller and Holly Langer, who reinforced my efforts by assisting me with many experiments; Simon Gruber and Bengt Svensson. I owe special thanks to Octavian

Cornea and Sarah Blakely, whose expertise in processing paperwork for grants, publications, and supplies was invaluable, saving me a lot of time, effort, and error. I thank Daphne Dong and Zhiwen Zhang for their help with the mass spectrometry that characterized my PLB standards, and I thank Ji Li for helping me out with the formatting of my thesis.

I thank my students, who taught me a lot about learning science through their questions, struggles, and achievements.

I thank my friends, who were invaluable through this process: Andrea Deese, Barbara Deese, Bob Deese, Nicole Fraser, Gary Fraser, Kathy Fraser, and Andrea Fraser, who treated me like family at critical times. Special thanks to Mike Mbughuni, my colleague in a neighboring lab, who helped me break the tension of lab work with the occasional Dairy-Queen blizzard. I thank Amber Eule-Nashoba, with whom I enjoyed several concerts and meals during my graduate career. I especially appreciated her knack for putting graduate school in perspective. I thank Miriam Ali for lots of good food and dancing. She also has a knack for putting many aspects of life in perspective. Thank you to Leighton Warmington, Endea Curry, Sheila Johnson, Adama Dinos, Eme Unanaowo, Candi Schulman, Ifrah Mansour, and all the members of the Black Graduate and Professional Students Association for your continued support.

I thank my committee: John Lipscomb, my committee chair, who guided me through my PhD with diplomacy and patience, and Gary Nelsestuen, James Fuchs, and Natalia Tretyakova, who provided support and encouragement.

Dedication

To my parents, Philomena Mensah and Emmanuel Ablorh, my sisters, Akweley, Akuorkor, and Tsotso, and most of all to Almighty God, who makes everything possible.

Abstract

Phospholamban (PLB) reversibly inhibits the sarcoplasmic reticulum calcium ATP-ase (SERCA) in cardiomyocytes. When SERCA is active, it pumps calcium into the sarcoplasmic reticulum (SR) to reduce cytosolic [Ca^{++}]. Calcium efflux from the cytosol reduces the Ca^{++} available to the cytosolic contractile apparatus so that the heart can relax during diastole. The extent of relaxation depends on the amount of calcium that SERCA removes from the cytosol during diastole, while the contractile force depends on the magnitude of the end-diastolic calcium transient. Thus SERCA inhibition affects both the contractile and relaxation phases of the cardiac cycle. Unphosphorylated PLB (uPLB) inhibits SERCA at low Ca^{++} concentration and phosphorylated PLB (pPLB) is less inhibitory, so myocardial physiology and pathology depend critically on the mole fraction of pPLB, X_p, equal to pPLB/(uPLB+pPLB), the concentrations of total PLB (tPLB) and SERCA, and uPLB/SERCA.

Prior to our assay, neither X_p nor tPLB could be measured accurately. Previous measurements relied on radioactive tracers, which only measured changes in these parameters, or immunoblots, which did not provide acceptable precision or accuracy. The fundamental problems with immunoblots were due to the lack of (a) accurate standards for pPLB and uPLB, (b) antibodies completely specific for pPLB and uPLB, and (c) a mathematical relationship between the antibody selectivity, the intensities of the samples and X_p. I have solved these problems using purified uPLB and pPLB standards, produced by solid-phase peptide synthesis, by performing two parallel immunoblots with antibodies partially specific for uPLB and pPLB, and deriving accurate equations for calculating X_p and tPLB. When this method was applied to mixtures of known composition, it measured both X_p and tPLB with ≥ 96% accuracy. I used this assay on samples of pig cardiac SR and found that X_p varied widely among four animals, from 0.08 to 0.38, but there was remarkably little variation in the ratios of X_p/tPLB and uPLB/SERCA, suggesting that PLB phosphorylation is tuned to maintain homeostasis in SERCA regulation. I have extended this method to measure accurately the mole fractions of PLB phosphorylated at Ser16, Thr17 and bisphospho-Ser16-Thr17 in biological samples, and to analyze the PLB phosphorylation status of cardiac tissue samples obtained from human patients with specific cardiomyopathies. This assay can

be adapted to any phospho-protein, and with any other posttranslational modification where purified standards and partially specific antibodies are available.

Table of Contents

List of Figures

List of Tables

List of Equations

List of Abbreviations

Ab, antibody

AFA-PLB, PLB that has been made monomeric by C36A- C41F-C46A-PLB mutations

ANOVA, Analysis of variance

app, the apparent, or measured value

ATP, adenosine triphosphate

BB, β blocker

cAMP, cyclic adenosine monophosphate

CaMKII, Ca^{++}/calmodulin-dependent protein kinase

CCB, calcium channel blocker

CD, circular dichroism

C_p, the concentration of phosphorylated phospholamban

CSR, cardiac sarcoplasmic reticulum

C_u, the concentration of unphosphorylated phospholamban

CV, coefficient of variance

C3b, complement

DAB, 3-3^{l} diaminobenzidine

DEER, dipolar electron-electron resonance

DTT, dithiothreitol

ECC, excitation contraction coupling

EDTA, Ethylenediaminetetraacetic acid

EDP, end diastolic pressure

EDV, end diastolic volume

EF, ejection fraction

EGTA, ethylene glycol tetraacetic acid

ELISA, Enzyme Linked Immuno-absorbent Assay

FMOC, Fluorenylmethyloxycarbonyl

FRET, fluorescence resonance energy transfer

FTIR, Fourier transform infrared spectroscopy

HDI, high-dose insulin (D50), 50% dextrose in water HR, heart rate

HPLC, high pressure liquid chromatography

HRP, horse radish peroxidase

Ig, immunoglobulin

IR, infrared

K_{Ca} the calcium concentration at ½ Vmax

KCl potassium chloride

K_{UP}, the measure of the antibody affinity for uPLB / antibody affinity for pPLB

MALDI-TOF-MS, Matrix-assisted laser desorption/ionization-time of flight mass spectrometry

MAP, mean arterial pressure

MHC, major histocompatibility complex

MOPS, 3-(N-morpholino)propanesulfonic acid

NMR, nuclear magnetic resonance

PBS, phosphate buffered saline

PISEMA, Polarization Inversion Spin Exchange at Magic Angle

PI3K, phosphatidyl inositol 3 kinase

PKA, protein kinase A

PLB, phospholamban

PMSF, phenylmethylsulfonyl fluoride

pPLB, phosphorylated PLB

pPLB/SERCA, mol/mol ratio of phosphorylated PLB and SERCA

PVDF, polyvinylidene difluoride

PP1, Phosphatase 1

PP1-I, Phosphatase 1 inhibitor

PP2A Phosphatase 2A 1

PP2B Phosphatase 2B

^{32}P, radioactive phosphate

REDOR, rotational-echo double resonance

RyR, ryanodine receptor

SDS, sodium dodecyl sulfate

SDS-PAGE, sodium dodecyl sulfate polyacrylamide gel electrophoresis

SEM, standard error of the mean

SERCA, Sarcoplasmic Reticulum Ca^{++}-ATP-ase

SR, sarcoplasmic reticulum

S16-pPLB, Phospholamban that is phosphorylated on Serine 16

tPLB, total phospholamban

tPLB/SERCA, mol/mol ratio of total PLB and SERCA

TBS, tris-buffered saline

TBST, tris-buffered saline with 1% Tween-20

TFA, triflouroacetic acid

TFE, triflouroethanol

TM, transmembrane

T17-pPLB, Phospholamban that is phosphorylated on threonine 17

uPLB, unphosphorylated PLB

uPLB/SERCA, mol/mol ratio of unphosphorylated PLB and SERCA

X_p, the fraction of total PLB that is phosphorylated

1. Chapter 1: Introduction

1.1 Significance

1.1.1 Phospholamban and Heart Disease

Heart disease is the leading cause of death in the United States. In 2008, it claimed over 616,000 American lives, accounting for almost 25% of deaths [1]. Heart disease is also an economic problem, costing $108.9 billion in 2010 [1] - more than any other diagnostic group [2, 3]. As of 2006, 5.8 million people in the United States were living with heart failure [3]. One in five heart failure patients will die within one year of their diagnosis [3]. Currently, the best hope of slowing this progression and increasing the chance of survival amongst patients is early diagnosis [1, 4].

The measurement of phospholamban (PLB) phosphorylation can aid in this early diagnosis. PLB is a cardiac protein that plays an integral role in cardiac health. It reversibly inhibits the sarcoplasmic reticulum calcium ATPase (SERCA) to impede Ca^{++} re-uptake after muscle contraction [6-8]. Unphosphorylated PLB (uPLB) inhibits SERCA while phosphorylated PLB (pPLB) attenuates SERCA inhibition [6] (Fig. 1). Since SERCA controls 70% of Ca^{++} flux in diastole in humans [8, 9], PLB expression and phosphoryl-ation are critical for Ca homeostasis, which ensures proper cardiac function during both systole and diastole in the cardiac cycle [10]. It has been shown that decreases in phosphorylation of PLB, increases in expression of PLB, and decreases in the expression of SERCA [9] lead to contractile dysfunction and heart failure [11]. Thus, augmenting PLB phosphorylation can provide treatment.

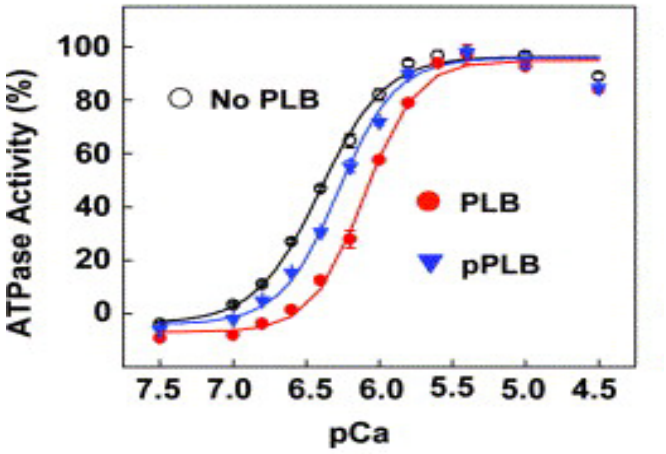

Fig. 1. PLB phosphorylation relieves SERCA inhibition. Black: no PLB, pK_{Ca} = 6.4. Red: PLB, pK_{Ca} [5] = 6.0. Blue: pPLB: pK_{Ca} = 6.3, so phosphorylation shifts the curve left to partially restore SERCA activity. Adapted from [6].

1.1.2 Significance of the Assay

This research describes the first method that accurately measures the mole fraction of PLB phosphorylation (X_p) and total PLB (tPLB). Together with the total SERCA level, these values have allowed calculation of the quantities uPLB/SERCA, pPLB/SERCA, and tPLB/SERCA. Establishing these ratios in patients without heart disease is paramount to establishing reference values to compare with those in subjects who have heart disease. They are essential in using PLB phosphorylation to chart the progression of heart disease, and in evaluating the efficacy of treatment strategies related to the PLB/SERCA complex in the heart Fig. 2.

1.2 Normal Cardiac Function

1.2.1 Normal Cardiac Cycle

The heart serves two physiological purposes. The right side Fig. 2 (blue) pumps deoxygenated blood to the lungs and the left side Fig. 2 (red) pumps oxygenated blood to the body. Each side of the heart has one atrium, one ventricle, an inflow vein and an outflow artery. Pressure gradients drive the blood flow between heart chambers and between the heart and the body. On the left side, oxygenated blood from the lungs flows into the left atrium, and then to the left ventricle. When it reaches the left ventricle, the muscle stretches so that the pressure is below that of the pulmonary vein, and blood is drawn into the ventricle. This is the relaxation phase of the cardiac cycle (diastole). Contraction of the myocardium (systole) reduces the volume in the ventricle such that the pressure in the ventricle is above that of the aorta, and

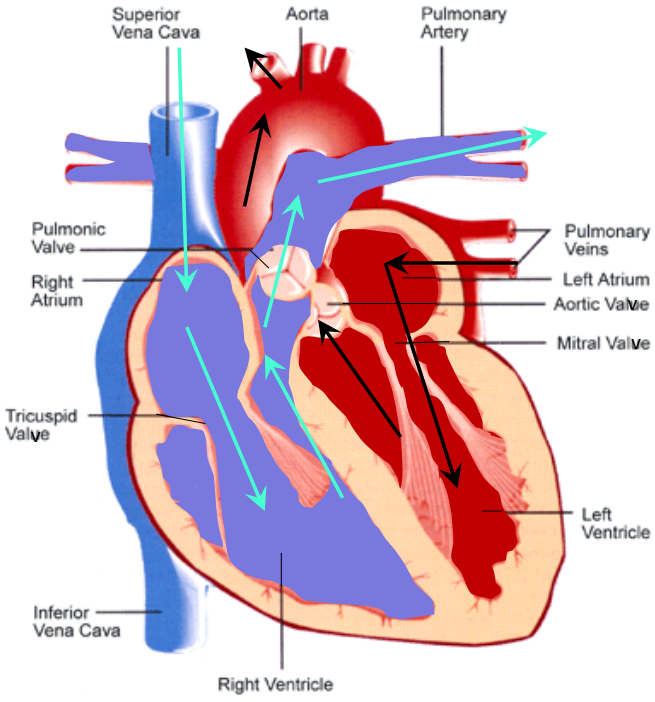

Fig. 2. Blood flow through labeled cardiac structures. Arrows symbolize the path on the left side (red with black arrows) and right side (blue with green arrows) of the heart. Adapted from [12].

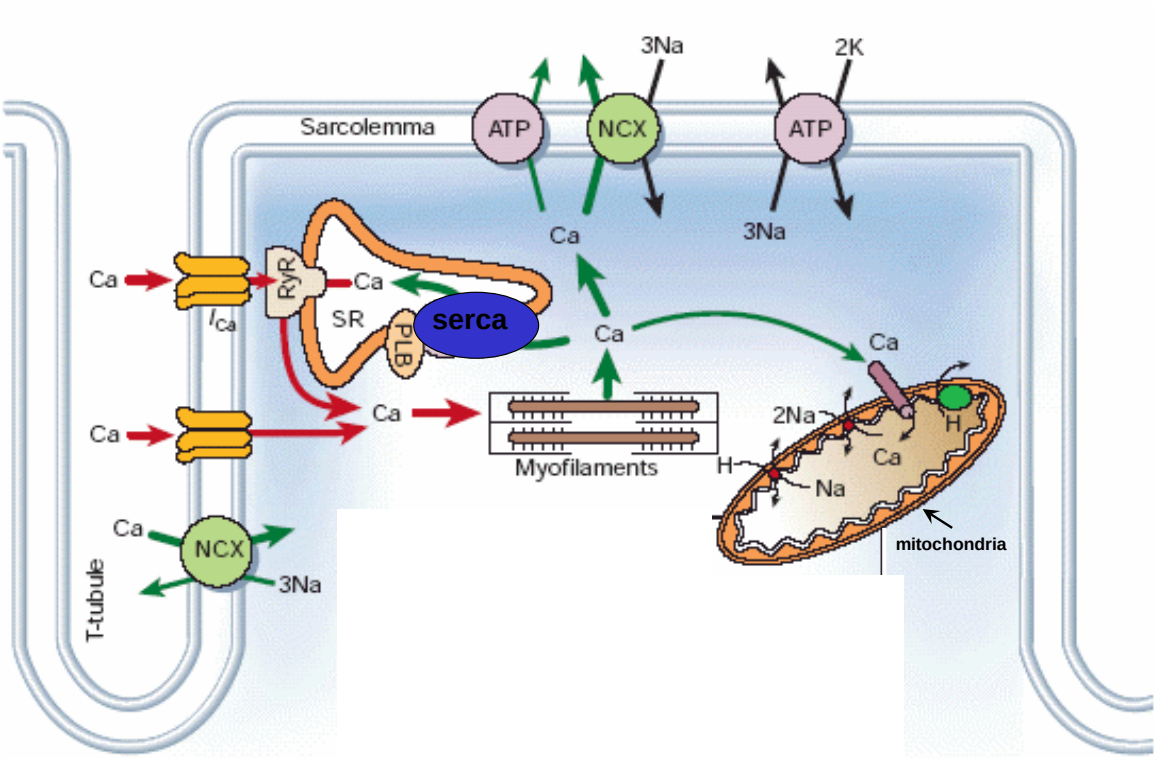

Fig. 3. Ca^{++} in contraction and relaxation.
Arrows represent the flow of Ca^{++} ions. Red arrows: cardiac excitation-contraction-coupling Green arrows: cardiac relaxation Yellow: L-type voltage-gated Ca^{++}channels. SR: (sarcoplasmic reticulum). PLB (phospholamban). Blue: SERCA (Sarcoplasmic calcium-ATP-ase) Green NCX (Sodium/Ca^{++} exchanger). Purple circle: ATP (sarcolemmal Ca^{++}-ATP-ase). Purple cylinder: mitochondrial Ca^{++} uniport. Myofilaments (the contractile apparatus, brown: myosin black:actin.). Adapted from [11].

blood is ejected from the ventricle into the aorta, the vessel that sends blood to the body [13]. Parallel events occur on the right side, where deoxygenated blood from the body enters the heart through the vena cava, travels to the right atrium, and to the right ventricle, and exits through the pulmonary artery to go to the lungs for oxygenation.

1.2.2 SERCA and PLB in Normal Cardiac Function

The heart beat is an involuntary, coordinated contraction, initiated by the action potentials of the sympathetic nervous system [14]. Transformation of the action potential to a contractile response is accomplished by excitation-contraction coupling (ECC) [11]. In ECC, excitation of the sarcolemma is coupled to contraction, the mechanical power stroke of the myofilaments (Fig. 3), by the movement of Ca^{++} between the cytosol and other cellular compartments [8, 11]. Thus, calcium homeostasis dictates both force and timing in the cardiac cycle. When the action potential reaches the t-tubules Fig. 3 of the myocyte, L-type voltage gated Ca^{++} channels Fig. 3 [11] open, causing a cellular influx of Ca^{++} [11, 14] from the outside of the cell. The influx of Ca^{++} calcium induces the release

of Ca^{++} from the sarcoplasmic reticulum, through ryanodine receptors [11, 14, 15] Fig. 3. This calcium is destined for the contractile apparatus.

The contractile apparatus, the sarcomere, contains actin, myosin, troponin, and tropomyosin. In order for the muscle to contract, the globular head of myosin must attach to actin and pull the actin filaments together to shorten the sarcomere [8]. However, without Ca^{++}, tropomyosin, a thread-like protein, conceals the myosin binding sites on actin [8]. When Ca^{++} binds to troponin C [11], tropomyosin exposes the myosin binding sites on actin [14]. Myosin binds to actin, and the actin-myosin cross-bridge cycling ensues. During the cross-bridge cycling, myosin heads deliver a power stroke that shortens the sarcomere. As long as Ca^{++} is bound to troponin, the muscle will continue to contract [8].

In order for the muscle to relax, the contractile apparatus must be calcium free [11]. To this end, the mitochondrial Ca^{++} uniport, sarcolemmal Na^{+}/Ca^{++} exchanger, sarcolemmal Ca^{++}-ATP-ase, and the sarcoplasmic reticulum Ca^{++} ATP-ase (SERCA) expel Ca^{++} from the cytosol Fig. 3. Of these pathways, SERCA is responsible for 70% of Ca^{++} re-uptake in humans [8]. Thus, increasing SERCA activity may also compensate for deficiencies in the other calcium-handling proteins. SERCA actively transports Ca^{++} into the SR [8] to facilitate muscle relaxation. The resultant Ca^{++} electrochemical gradient across the SR drives passive efflux of Ca^{++} in to the cytosol to initiate contraction [16]. uPLB-induced inhibition of SERCA impairs both relaxation and contraction. In the relaxation phase, uPLB prevents Ca^{++} -uptake into the SR, leaving the contractile apparatus exposed to Ca^{++} so that it cannot relax. During contraction, it depletes the electrochemical gradient of Ca^{++} across the SR so the muscle cannot contract. Phosphorylation of PLB restores SERCA activity [17] so that both relaxation [8, 11]. and contraction [14] can occur.

1.3 Cardiac Pathology

1.3.1 Heart Failure

The inability to pump enough blood to meet the metabolic demands of the body is defined as heart failure [14]. Heart failure is the destination of all progressive heart conditions, to include atherosclerosis, myocardial infarction, valvular stenosis, and cardiomyopathy. Cardiomyopathy refers to disease of the heart muscle itself, without participation from other organs. Dilated cardiomyopathy, where the ventricle is

permanently overstretched, is caused by systolic dysfunction. Hypertrophic cardiomyopathy, where copious thickening of the muscle permanently decreases the volume of the ventricle is caused by diastolic dysfunction. In restrictive cardiomyopathy, the stiffness of a normally sized ventricle prevents diastolic filling. Ischemic heart disease, sometimes referred to as ischemic cardiomyopathy, describes diseases of the coronary arteries, which can lead to either systolic or diastolic dysfunction [14].

1.3.2 SERCA and PLB in Heart Failure

When SERCA activity is impaired, stroke volume (stroke volume = end diastolic volume x ejection fraction) decreases and cardiac output (cardiac output = heart rate x stroke volume) is reduced: End diastolic volume (EDV) is the amount of blood in the ventricle at the end of diastole. Ejection fraction (EF) is the fraction of the EDV that the heart pumps out during systole. Through SERCA inhibition, uPLB reduces EDV by decreasing the stretch of the muscle fibers (the extent of relaxation of the muscle fibers) or decreasing the diastolic filling time (the duration of the relaxation phase) [18]. Lack of diastolic stretch due to SERCA impairment can also reduce the compliance of the ventricular wall so that end diastolic pressure (EDP) increases [13, 14, 19]. Then, the reduced pressure gradient between the veins and the ventricle causes retrograde filling of the veins, which is ultimately reflected in lower EDV [13, 14, 19].

SERCA impairment also affects the EF through the Frank -Starling mechanism. According to the Frank-Starling law of the heart, at low work-loads, the force of systolic contraction is directly related to the stretch of the cardiac muscle during diastole, which is reduced if SERCA is impaired [16]. At high work loads the EF is proportional to the contractility, which is reduced by decreases in the electrochemical gradient. The smaller the gradient, the fewer the number of sarcomeres recruited to maintain contractility [8, 11, 13, 14].

uPLB inhibits SERCA, precipitating the above decreases in diastolic stretch, diastolic filling time, and the electrochemical gradient that drives calcium release [11], with resultant decreases in cardiac output. Phosphorylation of uPLB [20] [17] and/or a decrease in tPLB expression [21] [22] [23] both attenuate SERCA inhibition [6] to increase or prolong SERCA activity, and maintain both passive stretch and contractility at a level compatible with life.

1.4 Phospholamban Structure and Phosphorylation

1.4.1 PLB Equilibria

PLB structure can be described by two, dynamic equilibria, a monomer vs. a homopentamer and a rigid, L-shaped T-state vs. a an extended, dynamic R-state [25] Fig. 4. In both the monomer and pentamer, the abundance of the T-state is >90% [26]. In the T-state, helix 1a Fig. 5 is perpendicular to the membrane normal [27] [28] and adheres to the membrane with its hydrophobic face [29]. In the R-state, helix 1a is detached from the membrane and extended so that it is approximately parallel to the membrane normal [30] Fig. 5. Endogenously, the PLB homopentamer predominates [31, 32], stabilized by leucine zippers [33] and 3 cysteine residues in the transmembrane domain [34]. The cysteine residues can be mutated to hydrophobic amino acids in order to stabilize a monomeric PLB. One such mutant, C36A- C41F-C46A-PLB, (AFA-PLB) [6], is depicted in Fig. 5.

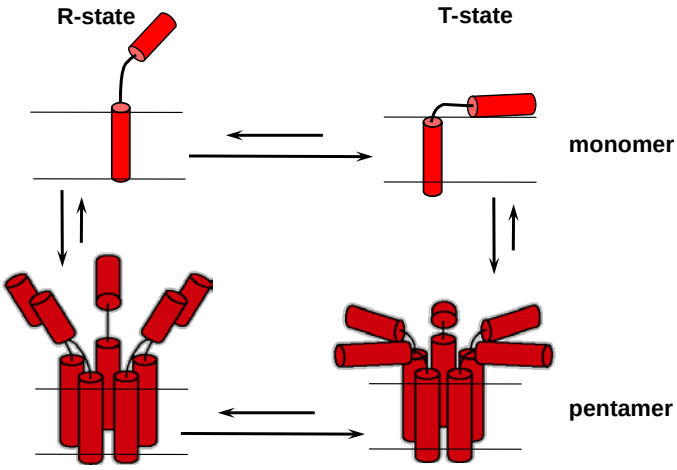

Fig. 4. PLB equilibria.
In the T-state/R-state equilibrium the T-state dominates in both monomeric and pentameric PLB. In the monomer/pentamer equilibria, the pentamer dominates in both the T-state and R-state equilibrium so that pentameric, T-state PLB is the dominant form. Adapted from [24].

1.4.2 PLB Monomer

Monomeric PLB is a 52 amino acid [36], single pass integral membrane protein that weighs 6KDa [36]. EPR and NMR [27, 29] studies have shown that PLB has 4 domains. They include Ia: an N-terminal amphipathic helix above the membrane (residues 1–16), the flexible loop: (residues 17–22), Ib: the part of the C-terminal helix that is exposed to the cytosol (residues 23–30), and II: the part of the C-terminal helix that is embedded in the membrane (residues 31–52) [29] [37]. Phosphorylation site S16 is located at the C-terminus of the cytosolic helix and phosphorylation site T17 is located at the N-terminus of the cytosolic loop [29] Fig. 5.

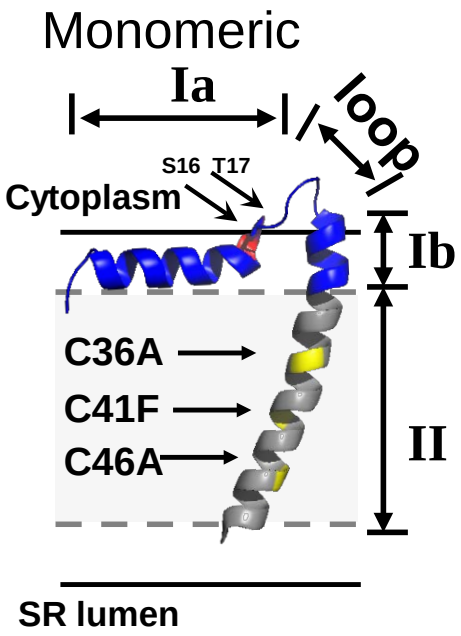

Fig. 5. Structure of the PLB monomer by hybrid NMR with identification of phosphorylation sites. Based on frame 12 from PDB 2KB7 [29] adapted from [35].

1.4.3 PLB Pentamer

Four models of the PLB pentamer were proposed; they diverge in their orientation of the cytosolic helix to the membrane normal. FTIR studies suggest an extended-helix sheet where the cytosolic domain is tilted 50-60^{o} from the membrane normal [38]. The continuous helix model proposed after rotational-echo double resonance (REDOR) and polarized FTIR revealed a cytosolic tilt of 28^{o} [39]; and triple resonance solution NMR suggests a 20^{o} tilt of the cytosolic domain [40]. All of the above resemble the R state. With the addition of in gel fluorescence resonance energy transfer (FRET) [41], dipolar electron-electron resonance (DEER) [38], polarization inversion spin exchange at the magic angle (PISEMA) [26], and hybrid solution/solid state NMR,. the field has converged on the pinwheel structure, which resembles the T-state [42], where the cytosolic domain is perpendicular to the membrane normal [26, 41, 42], and some of the

cytosolic residues are attached to the membrane surface [26, 42] as in the monomer above Fig. 5.

1.4.4 PLB Phosphorylation

PLB can be phosphorylated on one or both of residues S16 and T17 [43, 44]. PKA phosphorylates R-state PLB [45] at S16 in response to β adrenergic stimulation, which activates adenylyl cyclase, cAMP and then PKA Fig. 6. PKA subsequently phosphorylates PLB exclusively at S16 [46]. CaMKII exclusively phosphorylates T17 [46], but it requires supra μM Ca^{++} levels [44, 47]. Several in situ studies suggest that S16 phosphorylation is needed to relieve SERCA inhibition enough to elevate calcium levels in the cytosol to accommodate the Ca^{++}-dependence of CaMKII function [44, 48]. However, Kranias showed that T17 phosphorylation was greater than S16 phosphorylation in normal human hearts [49]. It is known that different etiologies of heart disease, such as hypertrophy [50] and acidosis [51] have elevated T17-pPLB where S16 PLB phosphorylation remained unchanged. CamKII phosphorylation also becomes important after sustained β1-adrenergic stimulation because prolonged or elevated CamKII activity [52] causes apoptosis of myocytes [53], and other deleterious effects [50], independent of PKA.

PKA and CamKII are both in competition with phosphatase 1 (PP1) Fig. 6, the major enzyme that dephosphorylates PLB [47], with phosphatase 2A and 2B playing a lesser role [55]. However, PKA counteracts PP1 when it phosphorylates PP1-inhibitor (PP1-I) at T35 [55-57]. Phosphorylation of PP1-I induces inhibition of PP1, PP2A, and PP2B [55] and maintains phosphorylation of PLB [58].

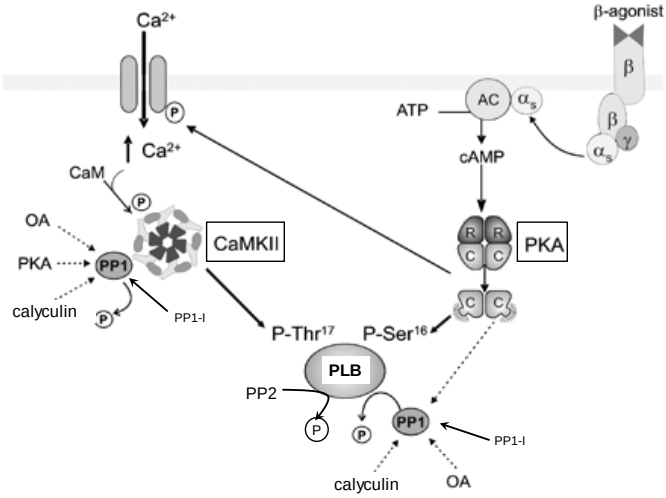

Fig. 6. PLB phosphorylation, dephosphorylation and phosphatase inhibition pathways.
β-adrenergic cascade (right) and CaMKII pathway (left). PLB is phosphorylated at S16 by stimulation of the β-adrenergic receptor (β) which activateds adenylyl cyclase (AC), cyclic AMP (cAMP) and then protein kinase A (PKA). PLB is phosphorylated by Calmodulin Kinase II (CamKII) in respose to high Ca^{++}. Phospatase 1 (PP1) and phosphatase 2 (PP2) dephosphorylate PLB at both sites. Okadaic acid (OA) and calcyculin inhibit PP1 and PP2 exogenously [54]. PPI-1 inhibits PP1 endogenously

When PLB is phosphorylated at S16, the phosphate forms a salt bridge with R13 [59] and also interacts with R14 [60]. This causes local unwinding of the cytosolic helix as shown by CD [61], solution NMR [62] and molecular dynamics simulations [59]. Phosphorylation of PLB thus provokes a hyperextension of the cytosolic helix that shifts the equilibrium from the T-state to the R-state [63]. Unwinding of the cytosolic helix also promotes dynamic disorder of the backbone of the whole cytosolic helix [62], causing it to move through an arc using the cytosolic loop as a hinge [64] Fig. 7.

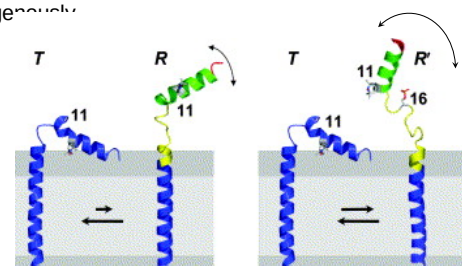

Fig. 7. Structural and rotational dynamics of 11-TOAC-AFA-PLB.
(a) uPLB equilibrium and (b) pPLB equilibrium Phosphorylation of PLB promotes both a shift in the equilibrium toward the R-state The pPLB R-state is hyper-extened and more dynamic (greater arc) than the uPLB R-state. Adapted from [6].

The physiological significance of the T to R transition is that the R-state PLB is much less inhibitory to SERCA than the T-state [6]. In fact, coaxing unphosphorylated PLB into the R-state with positively charged lipids relieves SERCA inhibition [65] while forcing phosphorylated PLB into the T-state with a lipid anchor [25] reestablishes SERCA inhibition [6].

1.5 SERCA

1.5.1 SERCA Enzymatic Cycle

SERCA is classified as a P-type ATP-ase because it is auto-phosphorylated (specifically at D351) during its reaction cycle [67]. Its function is to move 2 Ca^{++} per ATP [68, 69] from the cytosol to the lumen of the sarcoplasmic reticulum (SR) [70]. ATP hydrolysis provides the energy for SERCA to traverse several conformations in its catalytic cycle, in order to arrive at the E1 and E2 conformations. E1, which has a higher Ca^{++} affinity than the E2 conformation [71], facilitates Ca^{++} binding [72], and faces the cytosol [70] binds $2Ca^{++}$ molecules in the cytosol. The E2 conformation has a lower Ca^{++} affinity [71], and faces the SR lumen [70], facilitating Ca^{++} release into the SR [72] Fig. 8.

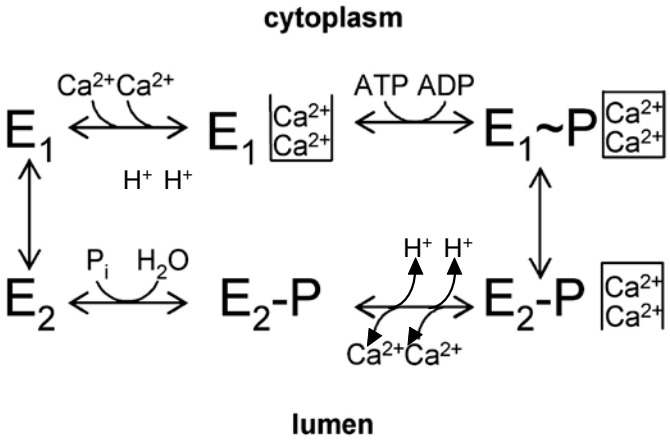

Fig. 8. SERCA enzymatic cycle.
The high Ca^{++} affinity E1 state binds two Ca^{++} ions. ATP hydrolysis provides the energy for the conformational change and autophosphorylation at D351 that take the high Ca^{++} affinity E1 to low Ca^{++} affinity E2-P. Ca^{++} is released into the lumen, and the phosphate is hydrolyzed from the E2 conformation. Adapted from [66].

With E1 facing the cytosol and having a high Ca^{++} affinity [71], it is poised to bind $2Ca^{++}$ ions from the cytosol, and then bind ATP. The $2Ca^{++}$- E1-ATP complex undergoes auto-phosphorylation to become $2Ca^{++}$- E1-P. The ATP hydrolysis drives two conformational changes. In the first, the Ca^{++} binding sites the Ca^{++}- E1-P are occluded [73]. At this point, the presence of ADP can drive the reaction backward to the ATP-bound state [70]. In the second, $2Ca^{++}$- E1-P flips so that the Ca^{++} binding sites are exposed to the lumen, and becomes $2Ca^{++}$- E2-P. During the transformation to the E2 state, SERCA is obligated to release $2Ca^{++}$ into the lumen of the SR [73], forming E2-P. For every Ca^{++} ion that is transported, 1 or 2 H^{+} ions are co-transported [73, 74]. After this, the phosphate is hydrolyzed to form E2, which is in a dynamic equilibrium with E1 [70] Fig. 8.

1.5.2 Structure and Isoforms of SERCA

The SERCA gene can be alternatively spliced to obtain SERCA1, SERCA2 and SERCA3 isoforms [75], which can be further subdivided into (SERCA1a-b, SERCA2a-d, and SERCA3a-f) [75]. However, some of the newly discovered subtypes correspond only to mRNA and not to actual protein [75].

SERCA1a, of fast-twitch skeletal muscle, is the archetypal SERCA [70], for which at least 44 crystal structures, representing different conformations and various ligand attachments are available [72]. The sarcoplasmic reticulum Ca^{++} ATP-ase isoform 1a (SERCA1a) is a 110KDa protein [72, 78] with 994 residues [68] that can be found in skeletal muscle. According to X-ray crystallography studies, SERCA1a is comprised of 4 domains: The actuator or anchor [73] domain (A), the nucleotide-binding domain (N), and the phosphorylation domain (P) face the cytosol and the transmembrane domain (M) Fig. 9.

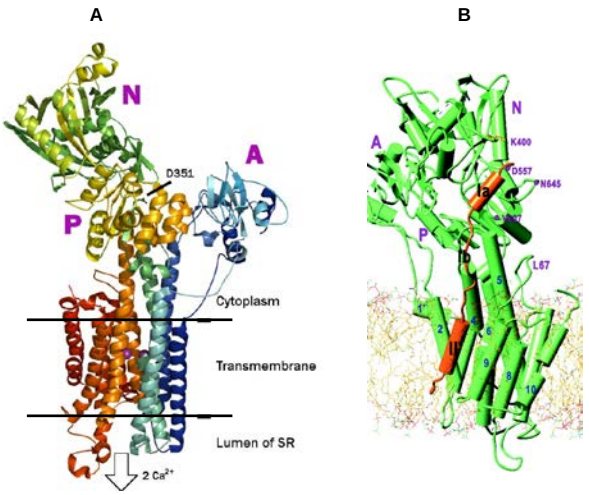

Fig. 9. Rabbit skeletal muscle SERCA.
(a) without PLB and (b) with PLB. In (a), the domains are labeled A, Actuator; N, nucleotide, P, phosphorylation, and M, transmembrane. D351, the phosphorylation site is labeled. In b, transmembrane helices are labeled 1-10, and PLB is docked onto the SERCA structure. K400, part of the analogous KGEKPV^{402} sequence essential to PLB binding to SERCA isoform 2a in skeletal muscle. Adapted from [76] (left) and [77] (right).

The A domain is the smallest domain, comprising several N-terminal amino acids. It floats on top of the M2 and M3 helices. The phosphorylation of D351 controls the Ca^{++} affinity of SERCA during binding and release. The N domain is a β-sheet surrounded by two helices that sits between the two β-sheets in the Rossman fold [67]. The P-domain forms a Rossman fold, in which the N-terminal and C-terminal β-sheets are separated by residues in the middle of the sequence, and the phosphorylation site (D351) is at the C-terminal end [72]. The transmembrane domain (M) consists of 10 α-helices connected by short, lumenal loops, except for the long loop between helices M2 and M3 [67]. In the M domain, the helices are of different lengths, and have different degrees of folding. Helices M1-M6 are clearly separated from M7-M10 [67]. The M-domain contains the two Ca^{++} binding sites in α-helices M4, M5, M6 and M8 [72]. Site I

is located in the space between helices M5 and M6 with a small contribution from M8 [67]. Site II is on M4 [67].

SERCA2a is the predominant SERCA isoform in cardiac muscle [75], and also in slow twitch skeletal muscle and smooth muscle [79] of several species [75]. SERCA2a and SERCA1a have ~ 84% sequence homology [79], and are functionally similar in their response to changes in PLB concentration in the cardiac tissue of transgenic mice [80]. However, SERCA1a exhibits greater V_{max} than SERCA2a [80] [81]. SERCA2a-d differ in the lengths of their C-termini (SERCA2a = 997 aa, SERCA2b = 1042 aa, SERCA2c = 999 aa, and SERCA2d = 1007). SERCA2b can be found in all tissues of several species, SERCA 2c may be unique to humans [75]. SERCA2c mRNA was found in hematopoietic cells [82], and SERCA2c protein was found in the heart [75, 83]. SERCA2c has a lower affinity for Ca^{++} than SERCA2a [83].

SERCA3 has 6 isoforms (a-f) that are found in both muscle and non-muscle cells, but none of them bind PLB [84].

1.6 PLB/SERCA Interactions

1.6.1 PLB Binding Domain on SERCA

Mutagenesis of SERCA2 has established that the phospholamban binds to amino acids 336-412 in the P domain of SERCA [84], with the tightest connections with the $KGEKPV^{402}$ sequence. Cross-linking studies suggest that the transmembrane domain of PLB binds near the M2 helix, with V49C PLB crosslinking to V89C-SERCA2a [85]. This is consistent with mutagenesis [77] and molecular modeling studies [86] of a PLB-SERCA1a interaction surface, in which PLB fits into a groove formed by helices M2, M4, M6 and M9.

1.6.2 The Mechanism of SERCA Inhibition by PLB

uPLB inhibits SERCA by decreasing its apparent Ca affinity (K_{ca}) [87]. Though a recent study of PLB in 2D crystals suggests that the PLB pentamer binds SERCA at an accessory site [88], EPR [32, 89], fluorescence [90] and mutagenesis studies [31, 91, 92] have lead to wide acceptance of monomeric, R-state PLB, as opposed to monomeric, T-state, or pentameric PLB as the primary inhibitor SERCA [6].

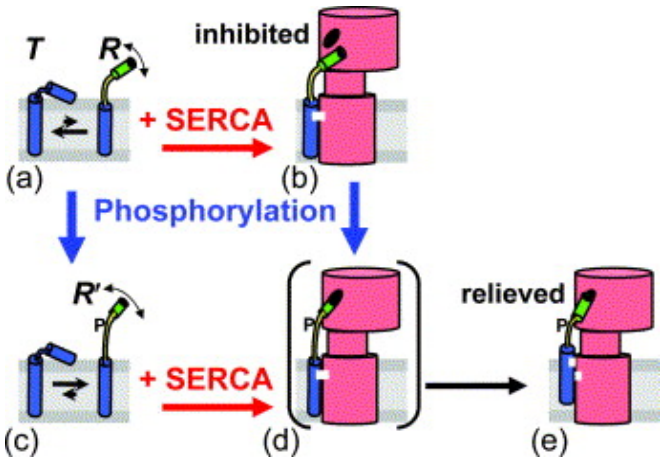

Fig. 10. SERCA inhibition and relief of inhibition by PLB. (a) T-state/R-state equilibrium of uPLB. (b) R-state binding to SERCA. (c) T-state/R-state equilibrium of pPLB where R-state has greater extension and dynamic range (called R^{I}). (d) RI-state pPLB binds to SERCA and relieves inhibition. Figure from [6]

1.6.3 Relief of SERCA Inhibition by PLB

Biological events that relieve SERCA inhibition include phosphorylation at S16 by PKA [93] Fig. 6, phosphorylation at T17 by CamKII [94] Fig. 6, decreased overall PLB expression [21], supra-micromolar [Ca^{++}], and PLB oligomerization. PLB phosphorylation at S16 hyper-extends the cytosolic domain to the R^{I}-state. In the R^{I} state, the angle between the cytosolic domain and the membrane normal is increased [6] [95] so that pPLB evacuates the inhibitory site on SERCA, [6] without dissociation from the complex [6, 96] Fig. 10. Parallel studies of PLB phosphorylation at T17 are lacking. Supra-micromolar Ca^{++} concentration and PLB oligomerization [97] are bi-products of PLB phosphorylation.

1.6.4 PLB and SERCA-Related Therapies

PLB, PP1, and SERCA are targets for gene therapy. Administration of gene therapy with pPLB mimics has been successful in treating heart failure in animal models. For example, mimicking the charge of the phosphate at the S16 site by S16E mutation [98] relieves SERCA inhibition [96] and has rescued hamsters [99] from heart failure. Mimicking the R^{I}-state of PLB by P21G mutation [100], and by double glycine mutation along the loop [101], and mimicking the pentameric state of PLB [102] are promising

alternatives for gene therapy due to their success in competing with WT-PLB for SERCA binding [103] *in vitro*. However, in vivo studies are needed to determine counteractive cellular response to the mutants; Possibilities include upregulation, decreased phosphorylation, and increased depolymerization of endogenous PLB. PLB gene ablation [22] and transcriptional repression [104] have been used to increase contractility in rat cardiomyocytes. However, null PLB genotypes have caused lethal dilated cardiomyopathy in humans [105], suggestive that the optimal X_p in humans is non-zero, and that some degree of SERCA inhibition is required for normal cardiac function. Suppression of PP1, the phosphatase that dephosphorylates PLB in an effort to increase X_p, is also a goal of gene therapy [106]. Overexpression of SERCA has rescued animals from contractile dysfunction [9], and has stayed disease progression in patients in late stages of heart failure in phase II clinical trials [107, 108].

The use of small molecules to increase SERCA activity has also been attempted. Astragalosides, for example, increase pPLB concentration, thereby reversing the heart failure symptoms caused by left anterior descending artery ligation in rats [20]. Six new small molecules that increase SERCA activity have also improved contractility in cardiac myocytes [109]. Istaroxime, which stimulates SERCA2 has increased both lusitropy and inotropy in phase II clinical trials [110] [111].

1.7 Accomplishments of This Research

This research has accomplished the quantification of the absolute mole fraction of phosphorylated PLB (X_p) using densitometry and western blots, with non-specific antibodies: Conventional western blotting methods cannot determine X_p because they cannot account for the non-linear relationship between intensity and total PLB on western blot. Until now, changes in phosphorylation has only been measured in relative terms, thus it is difficult to make comparisons between blots or between studies. The gravity of these relative ratios is difficult to interpret. For example, a 3-fold increase in X_p could mean an increase from 5% to 15% or from 25% to 75% phosphorylation. Furthermore, the relative measurements are in error because they assume specificity of uPLB antibodies and a linear relationship between intensity and tPLB on western blot.

X_p values are essential to other PLB calculations. For example, PLB expression requires X_p calculations because the relationship between tPLB and intensity values depends on X_p [112]. Several studies have reported that tPLB was unaltered by cardiac insult [113-119], based on equal intensities for normal and pathological samples on western blot. However, when X_p differs between samples, equal intensities necessarily reflect different expression levels. X_p values allow the calculation of other parameters such as uPLB/SERCA, pPLB/SERCA, and tPLB/SERCA ratios, which allow correlations between PLB phosphorylation, PLB expression, and SERCA inhibition.

Chapter 2: Antibodies, Synthetic Standards, and Western Blots are all Required for Accurate X_p Measurements

2.1. Absolute vs. Relative X_p

Absolute X_p is the mole fraction of pPLB/tPLB, which can be reported as a value from 0 to 1. Previous studies have attempted to use western blots to measure phospholamban phosphorylation of a sample relative to a reference sample of unknown X_p and unknown tPLB concentration. In these measurements, the ratio of the intensity of the sample labeled with a pPLB-selective antibody to the intensity of the sample on a blot labeled with a uPLB-selective antibody is recorded for a reference sample, which is in the control group. The same intensity ratios are then measured for the experimental samples. The fold-increase or decrease in X_p from the reference (control) sample in comparison to the experimental sample is then reported [94, 113-117, 119].

Commercial primary antibodies selectively bind uPLB over pPLB. We have shown that this preferential binding leads to a decrease in the apparent tPLB as X_p increases. As X_p increases, the denominator decreases, and the fold-increase in X_p is exaggerated. Similarly, as X_p decreases, the tPLB denominator increases, and the fold-decrease in X_p is exaggerated Fig. 11. To accomplish accurate X_p measurements, we have used standards of known concentration and purity [120-122] [112] to quantify antibody sensitivity on western blots and equations to relate the antibody sensitivity to the intensities of the sample.

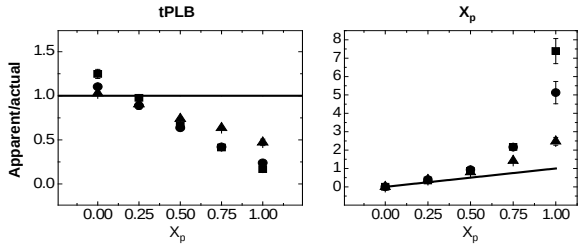

Fig. 11. Antibody selectivity affects the apparent tPLB and Xp in relative measurements.
(a) tPLB (b) X_p. square (Ab8A3) circle (Ab2D12), triangle (AbA1). In (a), the apparent/actual tPLB should be 1 because all samples have 12 ng of tPLB. In (b), the actual fold increase in X_p, using the X_p = 0.25 as a reference is represented by the linear curve.

2.2 X_p Techniques for the Measurement of PLB Phosphorylation

Though several methods are available to quantify phosphorylation of proteins, they are more costly, more limited in the biological systems to which they can be applied, less specific for the S16 or T17 sites, and less accurate than our method.

Radioactive phosphate has been used to study PLB phosphorylation [123]. ^{32}P cannot measure phosphorylation in cells and tissues because ^{32}P administered to live subjects could alter the endogenous phosphate before the X_p measurement. 1D-SDS PAGE/Pro-Q diamond/SYPRORuby is inexpensive, but not as specific as our method, as it cannot distinguish between phospho-proteins of equal molecular weight or between phosphorylation sites [124]. Phosphate –affinity SDS Page requires more expensive electrophoresis reagents, requires a pH of 7, and is more labor intensive [124]. Mass spectrometry requires several steps, including concentration of digested phosphoproteins on affinity columns, uses expensive instrumentation [125], and is not easily applied to membrane proteins. Sandwich ELISA requires two, specific antibodies, one recognizing only the phosphorylated part of the protein and another recognizing only the unphosphorylated part of the protein [126]. Our method may be applicable to conventional ELISAs, with the added benefit of high throughput screening.

Immunoblots are the method of choice to determine relative PLB phosphorylation [54]. A quantitative immunoblot was attempted in 2000, by Mayer et al. [120]. They reported a basal X_p as 4%, which increased to 17% upon isoproterenol stimulation. However, they concede that their standards were somewhat unreliable, that their method relies on an accurate measure of the total protein loaded. and that the accuracy of their measurements was compromised by the inability to represent antibody sensitivity in their calculations [120]. In an immunoblot, antibodies are used to bind protein targets.

2.3 Antibodies

2.3.1 Antibodies are Made by the Immune System

An antibody is a globular protein, also referred to as an immunoglobulin, and is a member of the acquired immune system [128]. In vivo, antibodies function to recognize foreign and pathogenic material for destruction [129]. When viruses, fungi or bacteria enter the body, they are engulfed by macrophages Fig. 12 or dendritic cells (not shown), which are both antigen-presenting cells [130]. An antigen-presenting cell digests the pathogen into fragments until one fragment, the antigen, binds to an MHC protein [128]. The antigen/MHC complex appears on the surface of the macrophage or dendritic cell in association with the class I or class II MHC proteins, prompting the macrophage to secrete Interleukin-1 (red dots and arrow) to activate the helper T-cells [128]. Then, the antibody-MHC complex binds to the receptors on helper T-cells in a specific interaction with the antigen. The T-cells secrete non-specific interleukins (green dots and arrow), comprising Interleukin-2, Interleukin 4 (B-cell growth factor, and interleukin-5, (B-cell differentiation factor). These factors stimulate the production of B-cells, which already contain antibodies (immunoglobulins) IgM on their Fig. 12 [128].

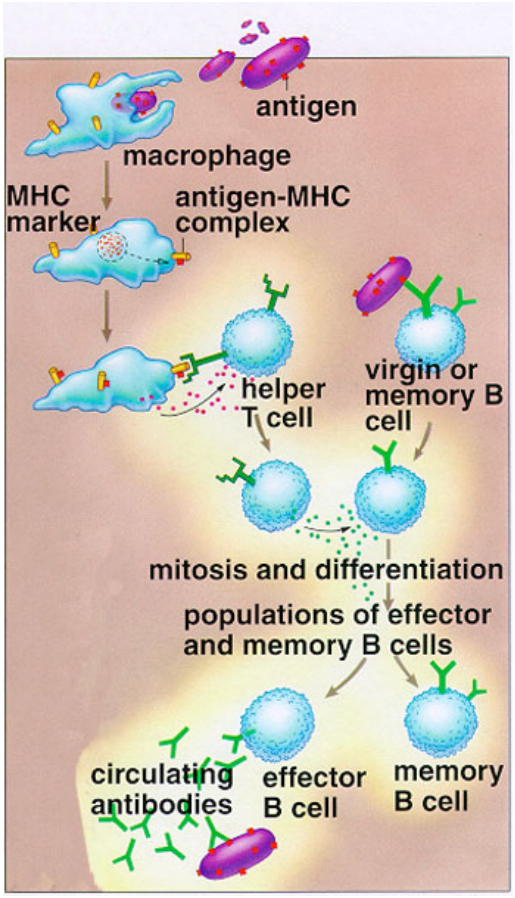

Fig. 12. Synthesis of circulating antibodies by the acquired immune system.
The macrophage engulfs the foreign particle and digests it until one of the fragments binds the MHC. The MHC appears on the cell surface, providing a receptor for the helper T-cell. The helper T-cell secretes interleukins (blue dots) that activate B-cells to differentiate into effector B-cells, which secrete antibodies into the blood. Figure from [127]

Each B-cell carries a different IgM on its surface that recognizes a specific antigen. The antigen will select the B-cell (clone) with the best-fit antibody on its surface. Antigen-binding to the membrane-bound antibodies stimulates the proliferation and differentiation of that B-cell clone into plasma cells that secrete the same specific antibodies into bodily fluids such as the blood stream, the ascites fluid, saliva and tears [128]. The antibodies then react with receptors on the surface of phagocytes to induce

digestion or activate complement (C3b), which also reacts with the phagocytic receptors. This is called active immunity because the antibodies are made in the host.

In the contrasting passive immunity, antibodies are produced by inoculating one host with a pathogen and transferring the antibodies to a second host. In this way, immunity is conferred to the second host. Passive immunity has many uses in medicine and basic research. For example, tetanus and botulism immunizations are the result of passive immunity, where the human is the second host [128].

2.3.2 Antibody Structure and Binding

An antibody is comprised of 2 identical heavy chains and 2 identical light chains, linked by disulfide bonds (Fig. 13) [131]. The heavy chains weigh ~ 60kDa. They contain 3 constant regions and 1 variable region. The light chains weigh ~ 25kDa, and have 1 constant region and 1 variable region. The variable regions of each chain have a hyper-variable region, comprised of 5-10 amino terminal residues form the antigen recognition site [128].

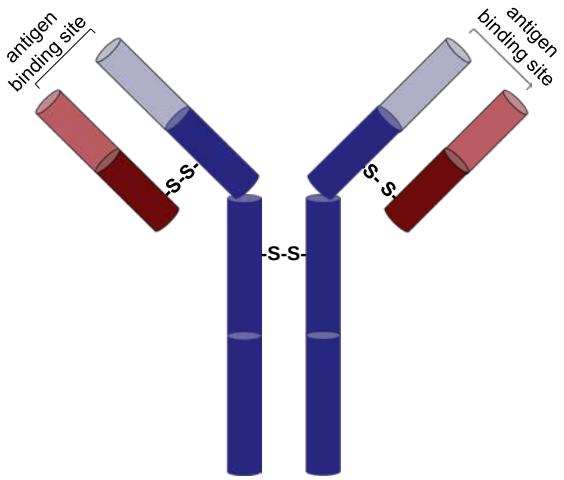

Fig. 13. Structure of an antibody.
The heavy chain (blue) has 1 variable region (light blue) and 3 constant regions (dark blue). The light chain (pink) also has a variable region (light pink) and 1 constant region (dark blue).The antigen binding site includes portions of the variable region of the heavy chain and light chain. The heavy chains and light chains are connected with disulfide bonds.

Antibodies are of 5 classes: IgA, IgD, IgE, IgG, and IgM that differ in the constant regions of their heavy chains. The B-cell-bound IgM antibodies are all monomers, but secretory IgA forms dimers, and secretory IgM forms pentamers, making them less attractive for laboratory research. Additionally, IgD is in low titer in the serum, and IgE easily forms crosslinks. Thus, IgG, which is a monomer in both its membrane-bound and secretory form, and is the most abundant class in the secondary immune response is commonly used for research purposes [128].

In vivo, antibody-antigen interactions are extremely specific because the antigen binding site (paratope), on the B-cells, have been programed, from birth, to bind only specific antigen epitopes [129, 130]. The antigen binds specifically, through hydrogen bonds, van der Waal's forces, and hydrophobic interactions. The number of non-

covalent interactions between the antibody and antigen determine the specificity of the antibody [128].

2.3.3 Antibodies in Basic Science Research

The properties of antibodies that are secreted into the plasma make them suitable for identifying proteins: The diversity of B-cell clones [132] makes antibodies suitable for almost any protein target. The specificity of one antibody to the protein target, which serves as the antigen, allows the identification of a target protein [128]. Antibodies can be labeled (with dyes) such that the number of proteins can be detected and quantified. Since antibodies are produced when any foreign material enters its host, they can be produced in large amounts by inoculating an animal host with a synthetic protein, a chemical, or an antibody from a different host [131].

To this end, antibodies against protein targets are raised in various mammalian species. The antigen for these antibodies can be a synthetic or recombinant peptide, attached to a molecular carrier [131]. The molecular carrier is required because the peptide is non-immunogenic. In other words, it can react with its specific antibody, but it cannot generate an immune response. The hapten cannot bind to the MHC proteins, and thus, cannot, by itself, be presented to the helper T-cell [128]. The epitope that the helper T-cell recognizes is on the carrier protein, and not on the peptide, but the B-cell recognizes the epitope on the protein [128].

In order to produce an antibody, the animal of choice must be inoculated with the protein once, to stimulate the primary immune response, and again, 3 weeks later [131], to stimulate a secondary immune response, generated by the memory B-cells created during the primary immune response [128]. During the primary immune response, the memory B-cell proliferates in anticipation of repeated exposure to the antigen. During the second exposure, the more numerous B-cells produce greater amounts of IgG [128]. The serum is then isolated from the blood by centrifugation, and called anti-serum [131]. The antibodies that are isolated from the anti-serum will be polyclonal: Polyclonal antibodies contain several different clones of B-cells for the same antigen [128, 131]. The variety of B-cells carry antibodies to a variety of epitopes, from different parts of the protein [128, 131]. As epitopes are only 5-10 amino acids long [131], some of these clones may also bind to epitopes on other proteins.

If instead, the antigen is injected into the spleen of a mouse or rabbit, and, after immunogenesis, the spleen is removed, the plasma cells from the spleen can be fused

to multiple a myeloma cell line to obtain a hybridoma (hybrid of the myeloma and B-cells). In this cell culture, each cell represents one clone, from which a monoclonal antibody titer can be achieved [128, 131]. The clones (B-cells) can be isolated using ELISA, western blots, or flow cytometry to retain the clone containing antibodies with the desired epitope, defined as monoclonal. Monoclonal antibodies are produced by only one B-cell. The monoclonal hybridoma can produce large amounts antibody and can be frozen and stored for multiple uses [128, 131].

Monoclonal antibodies are more useful in research than their polyclonal counterparts because they are specific to only one epitope on the target protein [128, 131]. However, if the epitopes on the target proteins are similar enough, varying by one conservatively mutated amino-acid side chain, or by a post-translational modification, cross reactivity may still occur. Thus quantitation of proteins with different isotypes or phosphorylation status may present the problem of antibody cross-reactivity.

Increased specificity can be accomplished by exposing the antigen to the host multiple times. With each exposure, somatic hyper-mutation occurs. In this process, the DNA of the paratope is mutated so that it conforms to the structure of the antigen epitope. The improved hyper-variable regions are more attractive to the antigen, and are selected more frequently than the previous antibodies [128].

Our method circumvents the problem of cross-reactivity with the use of protein standards, paired antibodies and linear equations [112].

2.3.4 PLB Antibodies and Epitopes

```
Human mekvqyltrs airrastiem pqqarqklqn lfinfclili cllliciivm ll
Rat   .......... .......... ......n... .......... .......... ..
Mouse .......... .......... ......n... .......... .......... ..
Dog   .d........ .......... ......n... .......... .......... ..
Rabbit.......... .......... ......n... .......... .......... ..
Pig   .d........ .......... ......n... .......... .......... ..
```

Fig. 14. Phospholamban sequences for different species.
The difference between the human sequence and the identical rat, mouse, and rabbit sequence is K2N, and the difference between human and identical pig and dog sequences are E2D and K27N.

PLB has been isolated in human, rat, mouse, dog, rabbit, pig, chicken, zebrafish, puffer fish, and recently in rainbow trout. Using the human sequence as a standard, rat, mouse and rabbit have K27N mutations. Dog and pig have E2D and K27N mutations. The epitopes for 2D12Ab, 285Ab, and A1Ab are known to be aa 9-17 for 2D12Ab, aa 7-

16 for A1Ab (Badrilla, Millipore), and aa 9-19 for 285Ab. The PLB standards synthesized for our experiment included pig uPLB, human uPLB, pig S16-pPLB, human S16-pPLB, human T17-pPLB, and human S16-T17-bis-pPLB. The epitopes for 2D12Ab, 285Ab, and A1Ab are known to be aa 9-17 for 2D12Ab, aa 7-16 for A1Ab (Badrilla, Millipore), and aa 9-19 for 285Ab. The epitope for P-17Ab (Santa Cruz) is proprietary, but it is 9 aa, including T-17. Thus, the epitope may include amino acids from aa 9-25. These epitopes occur outside the regions of mutation, so that human and pig pPLB and uPLB standards can be used interchangeably for X_p measurements in human, rabbit, rat, mouse, pig, and dog.

In western blots, S16 standards from either pig or human could be used interchangeably to measure X_p from any of the 4 animals because the mutations E2D and K27N do not affect the 285 epitope. Similarly, human-T17-pPLB or human S16-T17 –bis-pPLB standards from could be used to measure X_p from any of the 4 animals because the mutations E2D and K27N do not affect the P-17Ab epitope. The epitope for 8A3Ab has not been characterized. Therefore 2D12Ab was substituted for 8A3Ab for blots where X_p from pig species was calculated along with X_p from rabbit, mouse, and rat, because it is known that 2D12Ab does not bind in the region of the mutation sites E2D and K27N, and, unlike AbA1, does include the T17 phosphorylation site in its epitope.

2.4: Synthesis and Purification of Protein Standards

Synthesis of human or pig PLB was accomplished using automated FMOC solid-phase peptide synthesis of the appropriate sequence Fig. 14 as previously described [133], Manual incorporation of Fmoc-p-S16 and/or pT17 was verified by the ninhydrin test. Characterization was attained by MALDI-TOF-MS. Mass spectral data were acquired with a Bruker Biflex III matrix-assisted laser desorption/ionization time-of-flight (MALDI-TOF) system equipped with a N2 laser (337 nm, 3-ns pulse length) and a microchannel plate (MCP) detector. Data was collected in linear mode, positive polarity, with an accelerating potential of 19 kV. Each spectrum is the accumulation of 100–400 laser shots. The samples were co-crystallized with the matrix 3,5-dimethoxy-4-hydroxycinnamic acid (sinapinic acid).

The mass spectrum of acetylated wild-type uPLB is shown in Fig. 15. The apparent molecular weight was 6122 amu as compared to the actual molecular weight of 6123.5 amu, a difference of 1 amu, so the sample was extremely pure.

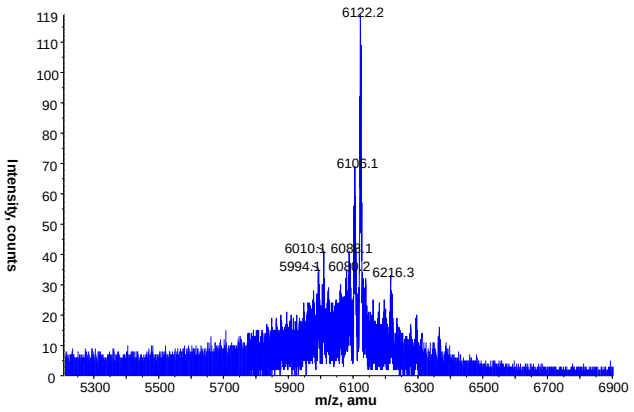

Fig. 15. Mass spectrum of acetylated wild-type uPLB.
The apparent molecular weight was 6122 amu

The mass spectrum of acetylated wild-type pPLB, phosphorylated at S16, residues 12-52 is shown in Fig. 16. The apparent molecular weight was 4849.6 amu as compared to the actual molecular weight of 4866 amu, a difference of 16 amu. The 16 amu difference most likely represents an oxygen atom.

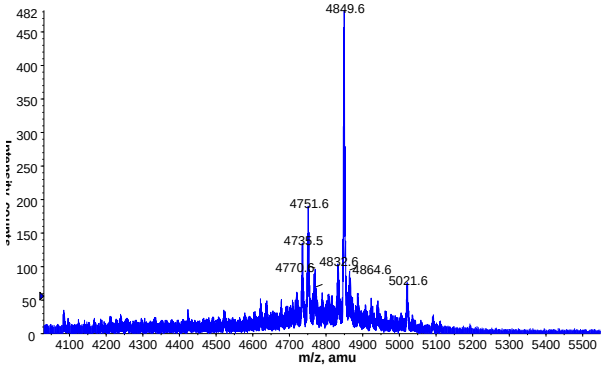

Fig. 16. Mass spectrum of acetylated wild-type pPLB, residues 12-52.
PLB was phosphorylated at residue S16.

HPLC purification was accomplished on a C-18 column (Vydac, 218TP54) with solvent A as water +0.1% TFA and solvent B as isopropanol + 0.1% TFA. The crude peptide was dissolved in 50% TFA. Peptide elution was achieved with a linear gradient. Fractions containing peptides were lyophilized to yield full-length PLB (15.4% yield based on starting resin) and TM–AFA–PLB (22% yield based on starting resin). After the lyophilization, the purified peptide was dissolved in of (tetra-methyl-flouro-ethanol) TFE Fig. 17.

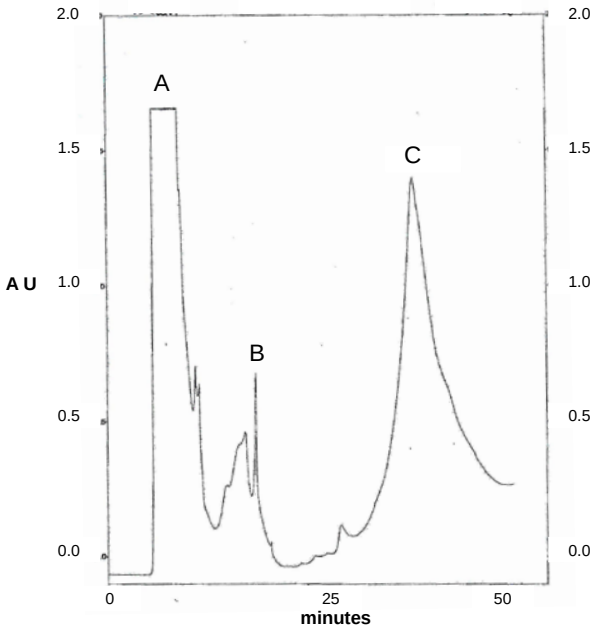

Fig. 17. HPLC of CH_3CONH-WT-PLB.
Peak A is the solvent A peak. Peak B is 30% CH_3CONH-WT-PLB. Peak C is the product, which is 76-100% CH_3CONH-WT-PLB.

2.5 Western Blot Method

1. Electrophoresis separates the proteins by molecular weight. Proteins are denatured, coated with negative charge by SDS, and then loaded onto a porous gel. If quantitation is desired, standards of known concentration of the target protein must be loaded at this step. A current is passed through the gel so that the proteins (negatively charged) travel toward the cathode. Larger molecular weight proteins travel slower through the pores, and thus travel a shorter distance than smaller molecular weight proteins. Proteins can thus be identified by their mobility shift (distance travelled)

The molecular weights of uPLB and pPLB are too similar for appreciable separation during electrophoresis Fig. 18, so more sophisticated techniques are required to distinguish between them. In mixtures of uPLB and pPLB, this negligible gel shift disappears because the uPLB and pPLB bands overlap. The gel shift between the uPLB and pPLB pentamers depends on the length of the gel, but the overlap depicted in Fig. 18 pertains to most commercial gels.

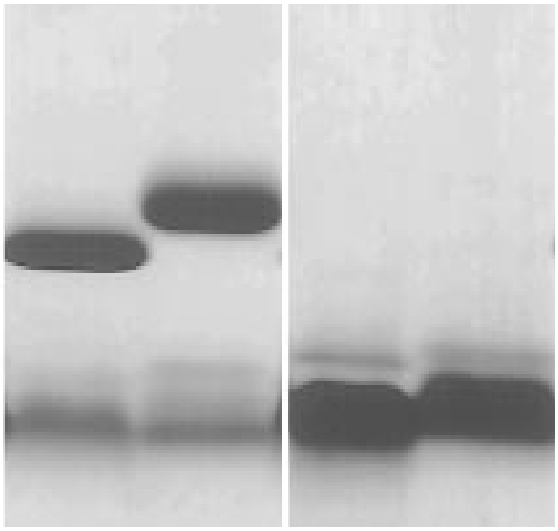

Fig. 18. SDS gel of recombinant PLB pentamer (A) and PLB monomer (B).
The small gel shift between the uPLB (left) and pPLB (right) pentamers disappears in mixtures where the bands coalesce. The uPLB (left) and pPLB (right) monomers will also coalesce if a mixture is electrophoresed. Figure from

Step 2: Proteins are transferred to a PVDF or nitrocellulose membrane with a current that runs perpendicular to the plane of the gel. In this step, all of the proteins on the gel are transferred to the membrane.

Step 3: Incubating the membrane in a blocking agent ensures that only the protein of interest will be labeled.

Step 4: Label with primary antibody. Ideally, the primary antibody is specific to the protein of interest. However, all of the commercial antibodies that bind to uPLB also bind to pPLB. If these uPLB antibodies bound pPLB with the same affinity as uPLB, then they could be used to calculate tPLB in a traditional, quantitative western blot, but all of them bind uPLB with a different level of preference. Primary antibodies are identified by the protein that they target and by the animal in which they were raised. For example, we used rabbit, anti-pPLB to label pPLB and mouse-anti-PLB to label uPLB Fig. 19.

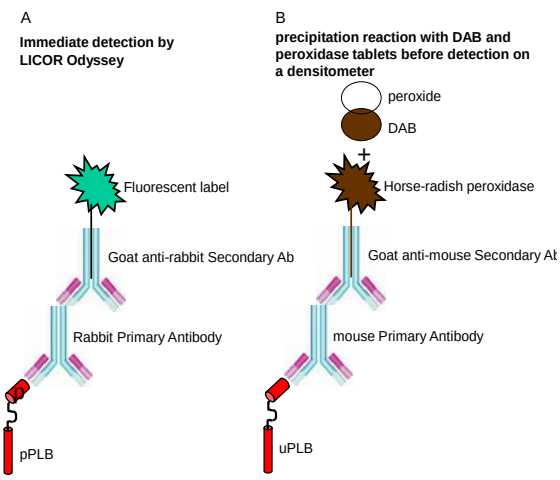

Fig. 19. Antibody labeling procedure for western blot.
A) and B) The primary antibody binds to the protein (PLB). Secondary antibody that is raised in the same animal as the primary antibody binds to the primary antibody. A) secondary antibody is attached to a fluorescent label. B) secondary antibody is attached to an enzyme (HRP) that catalyzes a precipitation reaction with

Step 5: Label with secondary antibody. The secondary antibody binds to the primary antibody. It can be from any animal, have been raised against the animal of the primary antibody. For example, the secondary antibody for mouse, anti-PLB must be an anti-mouse antibody in order that it binds to the primary antibody Fig. 19.

Step 6: Detect the intensity of the band on the western blot. The secondary antibody is conjugated to a means of detection, such as radioactivity, a precipitation reactant, or a fluorescent dye. We used di-amino-benzamidine-conjugated IgG (DAB-IgG) for one paper [134] and later switched to IR-dye-conjugated-IgG. DAB-IgG requires the addition of the enzyme horse-radish peroxidase (HRP) and peroxide after incubation with the secondary antibody. The HRP catalyzes a reaction between the DAB and the peroxide that leaves a brown precipitate at the site of the secondary antibody Fig. 19B. The reaction is stopped by the addition of water. The IR-dye-conjugated antibodies are ready for detection immediately after they are added Fig. 19B.

Step 7: Analysis by densitometry. Analysis of western blots is accomplished by densitometry. Due to the specificity of the primary antibody, visible bands are created only for the protein of interest. The other proteins are not detected because the primary antibody does not bind to them. The density of each band is recorded by the appropriate software. The relative density of the bands is proportional to the density of the secondary antibody, which is proportional to the concentration of the primary antibody, which is proportional to the concentration of the protein of interest. For a range of concentrations of protein and antibodies, this relationship is linear. Thus it is possible to compare the band densities in two different samples to determine their relative amounts of protein.

Because the uPLB antibodies are non-specific, this relationship is non-linear for uPLB. Since none of the PLB antibodies bind uPLB and pPLB with the same affinity, the relationship between the intensity of the uPLB + pPLB antibodies and tPLB concentration is non-linear Fig. 20. As a result of assuming that the above relationships are linear, qualitative measurements of changes in X_p and tPLB are exaggerated Fig. 20. The extent of these effects depends on the actual X_p of the sample, the affinity differential of the antibody, and on the incubation conditions. Thus, cross-study comparisons cannot be made.

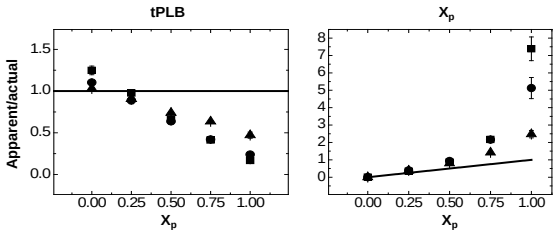

Fig. 20. tPLB measurements depend on X_p.
A) tPLB depends on X_p: as X_p increases, the intensity of the uPLB + pPLB antibody decreases, even though the amount of tPLB is the same because the antibody has a higher affinity for uPLB than pPLB. The result of this is that pPLB has a lower intensity reading than uPLB. **B)** X_p(app) is exaggerated as X_p increases because tPLB(app) (the denominator of X_p), appears to decrease. A) and B) The extent of these effects varies with the antibody chosen, because each antibody has a different affinity for uPLB. A1, (triangle), has the most equal affinity, followed by 2D12 (circle), followed by 8A3 (square).

Step 8 Quantitation by western blot: When the relationship between density and concentration is linear, a density vs. concentration curve (standard curve) can be constructed from the density of the standards of known concentration loaded in step 1. Then, the density of the samples can be interpolated to determine the concentration of the target protein in the sample.

The lack of a commercial antibody specific for uPLB or an antibody that is impartial to the phosphorylation state of PLB complicates X_p measurements. The measurement of X_p requires the concentrations of pPLB and uPLB, the concentrations of pPLB and tPLB, or the concentrations of uPLB and tPLB, but none of the antibodies available can measure either uPLB or tPLB independently. Thus, accurate and absolute X_p measurements require that both uPLB and pPLB standard curves are constructed for one blot, and that two such blots with two antibodies of different selectivity are performed. Then, a system of equations using the slopes of the 4 standard curves and the intensities of the samples is solved to obtain X_p. This method is detailed in chapter 4.

Chapter 3: Insulin-dependent Rescue from Cardiogenic Shock is not Mediated by Phospholamban Phosphorylation

3.1 Summary

We used immunoblots to determine whether inotropic and lusitropic effects of high-dose insulin (HDI) in cardiogenic shock, induced by a β blocker (BB) or a calcium channel blocker (CCB), are mediated by phosphorylation of phospholamban (PLB). PLB is a membrane protein that regulates calcium uptake into the sarcoplasmic reticulum (SR), by inhibition of the cardiac calcium pump (SERCA2a). Phosphorylation of PLB relieves SERCA inhibition, thus enhancing diastolic relaxation and preload. *Methods*: Our Institutional Animal Care and Use Committee approved this research. Swine myocardia from 6 groups were flash-frozen immediately upon death or sacrifice. Groups 1-6 received: (1) no medications, (2) HDI and glucose only, (3) toxic propranolol infusions and saline resuscitation, (4) toxic propranolol infusions and HDI resuscitation, (5) toxic verapamil infusions and saline resuscitation, (6) toxic verapamil infusions and HDI resuscitation. Groups 3-6 were resuscitated for 4 hours. Tissue samples from all 6 Groups were analyzed by quantitative immunoblots, using antibodies to both unphosphorylated PLB (uPLB) and phosphorylated PLB (pPLB), to determine the total PLB content and the fraction of PLB phosphorylated. *Results:* There were no differences in either pPLB or total PLB in cardiac tissue among any of the 6 Groups. However, infusion of a pig with the β-adrenergic agonist, isoproterenol, produced enhanced PLB phosphorylation. *Conclusion:* The mechanism by which high-dose insulin produces its inotropic and lusitropic effects in CCB- and BB-induced cardiovascular toxicity, resulting in resuscitation, is not due to changes in phosphorylation of PLB or a change in the total PLB in the sarcoplasmic reticulum (SR).

3.2 Introduction

High-dose insulin (HDI) is an accepted treatment modality in calcium channel blocker (CCB) and beta-blocker (BB) toxicity [135, 136]. Insulin is a well-known cardiac inotrope, and when used in the setting of CCB- and BB-induced cardiotoxicity, this effect is potent [137, 138]. The inotropic effects of insulin have been demonstrated in cardiac ischemia, cardiac surgery, and in sepsis-induced myocardial dysfunction [139-141]. Insulin also has positive effects on ventricular, diastolic relaxation (lusitropy) without changing myocardial oxygen requirements. In the systemic, pulmonary, and coronary vasculature, insulin functions as a vasodilator [142, 143]. The intracellular mechanisms of inotropy and lusitropy are unknown. In a canine model of verapamil toxicity, high-stressed myocardium heavily favored glycolysis over β-oxidation of the usual fatty acid substrate, to meet energy demands [138]. Insulin promotes cellular glucose uptake by activating glucose transporters on the cell membrane. Insulin increases glucose as an energy substrate during stress to improve myocardial energy production by: activating calcium and potassium channels, regenerating cytosolic ATP levels and enhancing aerobic metabolism [144].

Previous studies have shown that phospholamban (PLB) is the primary regulator of calcium uptake into the cardiac sarcoplasmic reticulum (SR), because it controls the cardiac calcium pump (SERCA2a), responsible for 70% of calcium uptake in humans [145]. In its unphosphorylated state, PLB inhibits SERCA2a, but phosphorylation of PLB relieves this inhibition. Increased SERCA function produces increased uptake of intracellular calcium into the SR, which promotes ventricular relaxation during diastole, and results in higher SR calcium stores [6]. The enhanced stretch of sarcomeres in diastole allows for increased pre-load, which may directly increase inotropy. Higher SR calcium stores allow for increased calcium release during contraction, also enhancing inotropy. PLB phosphorylation is primarily regulated via β-adrenergic stimulation of cAMP dependent PKA and Ca^{++}/calmodulin-dependent protein kinase [11, 145].

The phosphatidyl inositol 3-kinase (PI3K) pathway is one of the three major intracellular signaling pathways affected when insulin binds to its cell-surface receptor. It has recently been shown that verapamil toxicity can deregulate the PI3K pathway, and that HDI can re-activate the PI3K pathway, provided that insulin dosage far exceeds physiologic concentrations [146]. Cross-talk between the cAMP/PKA pathway and the PI3K pathway has also been shown [147]. It is unknown whether the inotropic/lusitropic

mechanism of HDI in CCB or BB toxicity is mediated ultimately by PLB phosphorylation and subsequent restoration of the cardiac, calcium pump (SERCA) activity [148]. Therefore, in the present study, we have used quantitative immunoblots, employing antibodies to both phosphorylated and unphosphorylated PLB, to determine whether HDI treatment, in these states of cardiogenic shock, is mediated by phosphorylation of PLB. Phosphorylation of PLB should result in positive downstream effects, including increased SERCA activity, greater calcium stores in the sarcoplasmic reticulum during relaxation, greater calcium transients in the cytosol during contraction, increased diastolic lusitropy and increased systolic inotropy. In previous studies, negligible changes in levels of PLB phosphorylation were detected in isolated pig SR membranes, subject to various cardiac challenges [149, 150]. However, it is possible that the time required to isolate SR membranes in these studies allowed endogenous phosphatase activity to mask changes in PLB phosphorylation. Therefore, in the present study, we analyzed flash-frozen tissue that was rapidly processed in the presence of phosphatase inhibitors, and we used positive controls to validate these procedures.

3.3 Methods

Surgical Protocols

Our Institutional Animal Care and Use Committee approved this research. Healthy, 12-week, Yorkshire pigs, weighing 27-35 kg, were sedated and anesthetized, during the entire protocol. Instrumentation included placement of a tracheostomy tube for ventilation, a pulmonary artery catheter placed via an internal jugular vein, femoral arterial and venous catheters, and another catheter in the urinary bladder. This enabled continuous cardiac output measurements, as determined by the thermodilution technique, as well as pulmonary artery and central venous pressure measurements. Arterial blood gas, pH, and mean arterial pressure were continuously monitored, and pCO2 was maintained near the baseline value. Nitrous oxide and isoflurane anesthesia were titrated by monitoring both reflexes and bi-spectral analysis values, to minimize cardiac depression. The heart was immediately harvested at the first of two events: mortality or the end of a 4-hour resuscitation protocol. Within 5 minutes, representative samples from the aorta, the walls of the left and right ventricles, and the intraventricular septum were flash frozen in liquid nitrogen, and stored at -80° C. A total of 12 pigs were divided into six groups, consisting of two each, as follows.

Negative Controls

Group 1 served as controls. These two pigs did not receive any medications, other than anesthesia for the purpose of harvesting tissue samples. Group 2 consisted of two pigs that received an insulin and glucose infusion for 4 hours. 2 units/kg/hr of insulin were infused at time zero, followed by an additional 2 units/kg/hr every 10 minutes, until a maximum of 10 units/kg/hr of insulin was reached, at 40 minutes. Glucose, in the form of D50, was infused and titrated to maintain this level at 60-120 mg/dl. Group 2 samples served as an additional control, and allowed us to study the effects of high-dose insulin and glucose, on normal pig hearts.

Reversal of Propranolol Toxicity with HDI-mediated Resuscitation

Group 3 and 4 both consisted of 2 pigs that received propranolol, but Group 3 was resuscitated with saline while Group 4 was resuscitated with HDI. An initial bolus of propranolol (0.5mg/kg) was administered. Then, propranolol was infused at

0.25mg/kg/min until toxicity was reached. Toxicity was defined as the time when the product of the heart rate (HR) and mean arterial pressure (MAP) decreased to 75% of the baseline product. At this point, the propranolol infusion rate was decreased to 0.125mg/kg/min, to simulate continued absorption of an oral overdose. In both groups, a normal saline resuscitation bolus of 20ml/kg of 0.9% saline was administered, over the next 10 minutes. This methodology has been used in previous models [137]. Group 3 continued a baseline saline resuscitation for 4 hours. However, HDI infusion replaced the saline in Group 4, titrating from 2 to 10 units/kg/hr. Glucose, in the form of D50, was infused and titrated to maintain a concentration of 60-120 mg/dl (as outlined in Group 2) and continued, until the first of death or 4 hours.

Reversal of Verapamil Toxicity with HDI-mediated Resuscitation

Group 5 and 6 both consisted of 2 pigs that received verapamil, but Group 5 was resuscitated with saline while Group 6 was resuscitated with HDI. In both groups, a verapamil bolus of 0.5 mg/kg/hr was increased by 0.5 mg/kg/hr every 10 minutes until the point of toxicity, defined as in Groups 3 and 4. At this time, the infusion rate was decreased by 50%. In both Groups, a normal saline resuscitation bolus of 20ml/kg of 0.9% saline was administered, over the next 10 minutes. Group 5 continued with a baseline saline infusion, until the first of death or 4 hours. Group 6 was given an insulin infusion, titrating from 2-10 units/kg/hr. Glucose, in the form of D50, was infused and titrated, with the goal of maintaining this level between 60-120 mg/dl, as outlined in Group 2 and Group 4, and continued until the first of death or 4 hours.

Tissue Extraction

Frozen tissues were extracted at 4^{o}C in a buffer containing 2% SDS, 1mM PMSF, 1mM Benzamidine, 10mM NaF, 1mM DTT, 1mM EDTA, 1mM EGTA and 50mM Tris-HCl (pH 7.2). 2nM calyculin was added to extraction buffer just prior to use. 1g of tissue was cut with a knife, and homogenized in 5mL of extraction buffer with a polytronic homogenizer. The homogenates were centrifuged at 15,000g (11,200 rpm in an SS-34 rotor) for 10 minutes, and the protein-containing supernatant was stored at -20^{o}C (short-term), and at -80^{o}C (long-term). This extract represented more than 60% of the total protein, as measured by the biuret assay, using bovine serum albumin as a standard.

SDS-polyacrylamide Gel Electrophoresis (SDS-PAGE) and Western Blot

Electrophoresis was carried out on a Criterion apparatus (Bio-Rad), on 15% polyacrylamide, containing 0.1% SDS slab gels (1.5mm thick), using the discontinuous buffer system of Laemmli [151]. Samples (40μg) were mixed in a 1:1 ratio with sample buffer (125mM Tris-HCl, pH 6.8, 4% SDS, 20% glycerol, 10% β-mercaptoethanol, 0.01% bromophenol blue), and boiled for 2 min. before loading the sample on the gel. Standards of unphosphorylated PLB (uPLB) and S16-phosphorylated PLB (pPLB) were prepared by solid-phase peptide synthesis [152]. Prestained, broad- range protein molecular weight SDS-PAGE standards (Bio-Rad), with molecular mass ranging from 7 to 205 kDa, were used as standards. The samples were electrophoresed at constant voltage (100V), for 80 min.

Western Blot Detection of Phospholamban

The proteins separated by electrophoresis were electro-transferred to PVDF membranes (Bio-Rad), according to the method of Towbin et al [153]. The western blot transfer was performed in the presence of Tris-glycine buffer (25mM Tris, pH 8.3, and 192mM glycine, containing 10% methanol), in a Transblot cell (Bio-Rad), at 280 mA constant current, for 50 min at 4°C. The membranes were blocked with 2% non-fat dry milk, for 1 hour, and then washed for 10 minutes, 3 times, with PBS, containing 0.1% Tween 20. The membranes were incubated with either of two primary antibodies, 1D11Ab or 285Ab, in blocking buffer. Anti-PLB monoclonal antibody 1D11, binds both phosphorylated and unphosphorylated PLB. Anti-phosphoserine PLB polyclonal antibody 285, which only binds PLB phosphorylated at serine 16. Both were produced and purified as described previously [154]. 1D11Ab or 285Ab (7.2mg/mL) was diluted between 1:2000 and 1:3000. After 1 hour incubation, excess primary antibody was washed for 10 minutes, 3 times, with PBS, containing 0.1% Tween 20. The blots were subsequently incubated with secondary antibodies. 1D11 was incubated with 1mg/mL stock solution of horseradish peroxidase-conjugated goat anti-mouse IgG (H+L)-HRP (Southern Biotech. Associates, Inc.), diluted between 1:1000 and 1:2000, in blocking buffer, without sodium azide, for 1h, at RT. 285Ab was incubated with goat anti-rabbit IgG –HRP (Sigma), diluted between 1:1000 and 1:2000, in blocking buffer, without sodium azide, for 1h, at RT. Excess secondary antibody was washed for 10 minutes, 3 times, with PBS, containing 0.1% Tween 20. The antigen-antibody complexes were visualized by staining for

peroxidase activity with 3, 3' diamino-benzidine tablets (DAB) (Sigma), as a substrate. The color-reaction was stopped by washing with deionized water. The immunoblots were scanned by a densitometer, using the reflectance mode, and the bands were quantitated using the volume (area x density) analysis method.

3.4 Results

Validation of Methodology

We first performed control experiments to demonstrate that we can detect uPLB and pPLB in porcine cardiac tissue. Synthetic, unphosphorylated PLB (uPLB) and phosphorylated PLB (pPLB), were used as standards (first six lanes of Fig. 21). 285Ab only detects pPLB (Fig. 21 top), while 1D11Ab detects both uPLB and pPLB, with a slight preference for uPLB (Fig. 21, bottom). Both antibodies have approximately linear sensitivity in the range of 6 to 25 ng of PLB. Thus, 285Ab and 1D11Ab provide accurate measures of pPLB content and uPLB content, respectively. Our ability to detect both forms of PLB in porcine cardiac tissue is illustrated in the right two lanes of Fig. 21, which represent samples taken from the right ventricles of control pigs. For the pig that was given no medications ("-"), negligible pPLB, equal to or below the background, was detected (Fig. 21, top), but the total PLB was substantial (Fig. 21, bottom, 17.50 ng PLB/μg). Thus, less than 1% of PLB was phosphorylated, for the pig receiving no medications. As a positive control, another pig was given isoproterenol, which is known to induce phosphorylation of PLB via the β-adrenergic receptor, with downstream signaling through protein kinase A (PKA) [155, 156]. The pig received isoproterenol 5 μg/min for two hours, resulting in the

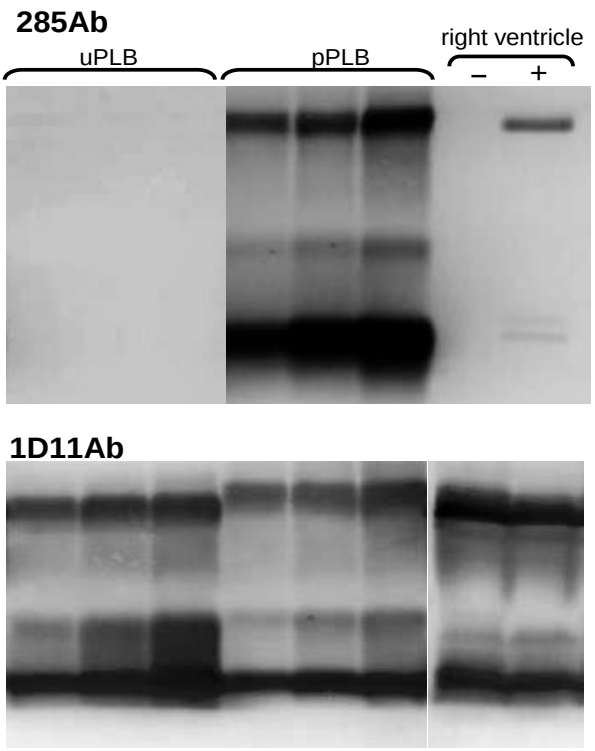

Fig. 21: Western immunoblot, isoproterenol control. Primary antibodies are 285Ab (top, specific for pPLB) and 1D11Ab (bottom). Lanes 1-6 are synthetic uPLB and pPLB standards (6 ng, 12 ng and 25 ng). For tissue samples, "-" indicates no medications, while "+" indicates isoproterenol administration (see text).

HR increasing from 90 to 175/min. The pig was sacrificed, and the cardiac tissues were harvested and analyzed, as described in Methods. Isoproterenol had no significant effect on the total amount of PLB, in the right ventricle (Fig. 21, bottom right, "+"), but it did produce a significant level of pPLB (Fig. 21, top right, "+"), corresponding to 1.1 ng/μg total protein, showing that 6.25% of the PLB was phosphorylated.

Pig Survival Data

Although survival was not a study aim, both pigs in Group 2 (insulin and glucose alone) survived for 4 hours. In Group 3 (propranolol and saline), one pig died after 86 minutes of resuscitation and the other survived for 4 hours. In Group 4 (propranolol and HDI), both pigs survived for the total 4 hours of resuscitation. In Group 5 (verapamil and saline), both pigs died; one at 60 minutes, the other after 105 minutes of resuscitation. In Group 6 (verapamil and HDI), one pig survived the 4-hour resuscitation. The other died at 210 minutes. In summary, 3 of the 4 pigs resuscitated with HDI survived, and 1 of the 4 saline-resuscitated pigs survived.

Resuscitation from Cardiogenic Shock

Fig. 22 demonstrates results of the average cardiac output measured for two pigs from each group during 4 hours of resuscitation. Time "0" on the X-axis is the point of toxicity as defined in methods, and the data from each group was standardized to 100% (baseline) for easier interpretation of the data. Group 1, given no medications, is not shown, because it was used to establish the baseline for pPLB in Fig. 23 and not to establish baseline cardiac output. The cardiac output control (Group 2, Fig. 22, black) was given only HDI and glucose, without induced

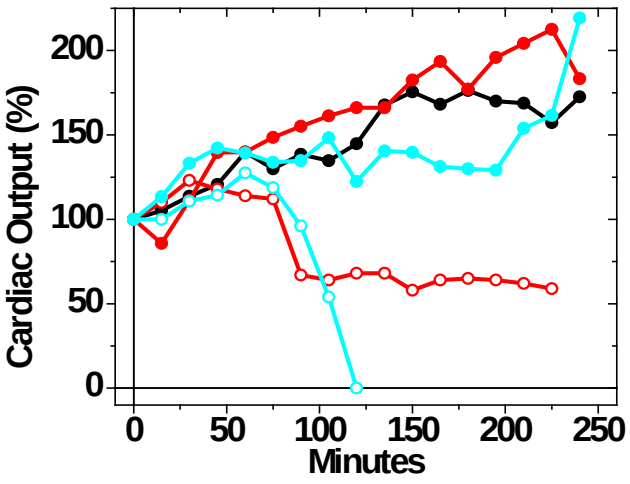

Fig. 22: HDI improves cardiac output after toxicity. Cardiac output (L/min), expressed as % of the value at time 0 (point of toxicity, as defined in text), at which resuscitation was begun with either saline (open symbols) or HDI (closed symbols). Black: control (HDI and glucose only). Red: toxicity induced by propranolol. Cyan: toxicity induced by verapamil.

toxicity. Groups 3 and 4 (red) show that propranolol induces severe toxicity, which is reversed by HDI/glucose resuscitation, as reported previously [137]. The curve for Group 3 (red, open circles) is likely high, due to inadvertent excess saline administration, during resuscitation phase, in one of these pigs. Groups 5 and 6 (cyan) show that verapamil induces severe toxicity, which is reversed by HDI/glucose resuscitation. The results show clearly that resuscitation with high-dose insulin can rescue porcine myocardia from BB- and CBB-induced cardiogenic shock, as evidenced by the return of cardiac output to a level comparable to that of controls.

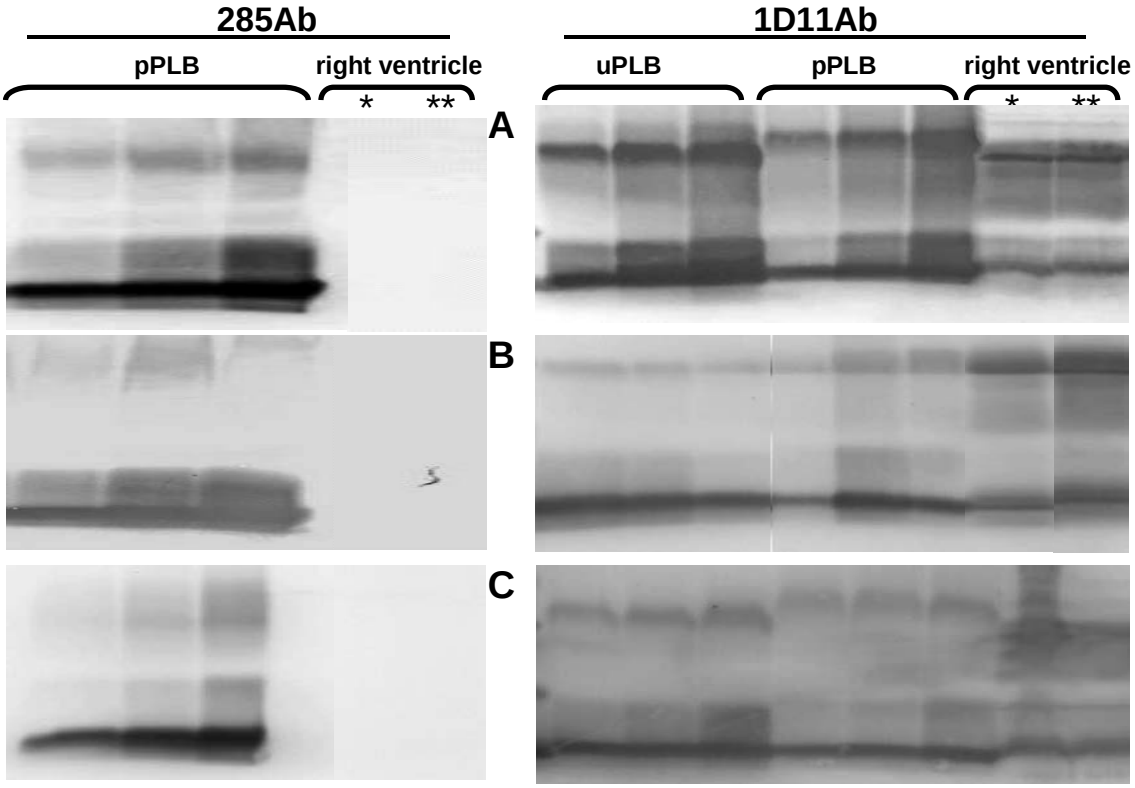

Fig. 23: **Western immunoblots of samples in Groups 1-6. Left: 285Ab.**
Right (285Ab as shown in Fig. 21). Lanes 1-3: synthetic pPLB standards. Right: 1D11Ab, Lanes 1-3, synthetic uPLB standards. Lanes 4-6, synthetic pPLB standards. For right ventricular tissue samples, A: * normal control (Group 1), ** insulin and glucose (Group 2). B: * * propranolol only (Group 3), ** propranolol and insulin (Group 4), C: *verapamil only (Group 5), ** verapamil and insulin (Group 6).

Immunoblots from Groups 1-6.

Immunoblots were performed on harvested cardiac tissues. Because PLB content was consistently found to be highest in the right ventricle, analysis focused on those samples. The total PLB content, measured with 1D11Ab, was essentially unchanged (4.4 ng/μg) by any of the treatments (Fig. 23, right). Tissues were evaluated for their pPLB content by immunoblot, with Ab285 (Fig. 23, left). Fig. 23A shows that phosphorylated PLB (pPLB) was not significantly above background, in the samples corresponding to Group 1, normal control (*), and Group 2, insulin plus glucose (**). Fig. 23B shows that there was no change in pPLB after either inducing cardiogenic shock with propranolol (*), Group 3, or treating propranolol-induced shock with HDI (**), Group 4. Similarly, Fig. 23C shows that there was no change in pPLB after either inducing cardiogenic shock with verapamil (*), Group 5, or treating verapamil-induced shock with HDI (**), Group 6. Similar results were obtained for the other four tissues studied. In summary, propranolol-induced cardiogenic shock, verapamil-induced cardiogenic shock, and HDI-mediated reversal of cardiogenic shock all failed to affect PLB content or PLB phosphorylation.

In light of the surprising observation that pPLB was observed only in the case of isoproterenol treatment (Fig. 21), we performed control experiments to determine whether the results were affected by phosphatase activity during tissue extraction. Synthetic pPLB (25 ng) remained reactive to antibody 285 even after 1 hour incubation with tissue-extract-containing phosphatase inhibitors at 37°C (not shown). Thus, PLB phosphorylation was not masked by endogenous phosphatase activity.

3.5 Discussion

Several previous studies have sought to determine the underlying mechanisms of the inotropic properties of insulin therapy on the heart. Initial work, looking at these effects in toxicity-induced myocardial depression from CCB and BB toxicity, has focused on myocardial energy-substrate mechanisms, including glucose and lactate uptake, and pyruvate dehydrogenase activation. Under normal conditions, the heart uses primarily free fatty acids, which account for 80% of ATP production [157]. Under conditions of stress, glucose becomes the preferred substrate. Insulin, in high doses, dramatically increases intracellular glucose transport in cardiogenic shock, and is associated with increased inotropy [158]. This process is activated by mitogen-activated protein kinase, a major intracellular insulin-signaling pathway [146]. Translocation of GLUT 4 complexes to the cellular membrane is induced by insulin by both GTPaseTC10 activity and the PI3K

pathway [159]. Glucose can also be transported into myocardial cells by the less abundant GLUT 1, which is not insulin sensitive, and allows for glucose uptake, in the absence of insulin [157]. Previous work in BB-toxic pigs, demonstrating insulin in doses up to 10 units/kg/hour, markedly increases cardiac output to levels greater than measured in the resting, pre-toxic state, led our group to hypothesize that mechanisms other than energy-substrate and metabolism may be involved in this process [137].

Intracellular calcium is essential for cardiac, electrical activity, and is the direct activator of the myofilaments that cause myocardial contraction. Events that lead to calcium mishandling in the cell are primary causes of contractile dysfunction in the heart [11]. The abrupt rise in free, intracellular calcium comes primarily from Ca^{++} influx, through the L-type calcium channels, during the action-potential. This triggers calcium release from the sarcoplasmic reticulum, through its release channels, the ryanodine receptors (RyR). Ventricular relaxation is primarily under control of PLB, which regulates the uptake of free calcium, back into the SR, by SERCA2a. The most direct and potent control of PLB is through activation of the β-adrenergic receptor, by which adenyl cyclase increases cyclic AMP (cAMP). cAMP, in turn, activates protein kinase A (PKA) [160]. PKA phosphorylates several proteins, including PLB, RyR, L-type calcium channels and troponin I. Phosphorylation of PLB is the predominant mechanism of increased lusitropy, mediated by accelerating SR calcium uptake [161]. PLB phosphorylation increases inotropy by recovering the function of SERCA2a, which pumps calcium into the SR from the cytosol, thus increasing SR calcium stores. When calcium stores are released, during muscle contraction, the calcium transient is increased, with a resultant increase in the force of cardiac contraction.

Activation of the β-adrenergic receptor, with subsequent activation of PKA and phosphorylation of PLB at Serine-16, results in relief of SERCA inhibition [160]. PLB can also be phosphorylated at Threonine-17, in response to activation of Ca^{++}/calmodulin-dependent kinase II, which may also be modified by β-adrenergic stimulation [114, 160]. However, serine-16 is the predominant site of PLB phosphorylation, both at baseline and after cardiac challenge [150, 154]. 285Ab is specific for phosphorylation of phospholamban at serine-16. Future studies with antibodies specific for threonine-17 phosphorylation will be illuminating.

Cross-talk between the PI3K and the cAMP/PKA pathway has been established [162]. Moreover, the effect of PI3K signaling on cardiac contractility may require activation

of the cAMP/PKA pathway [147]. Conversely, inhibition of PI3K signaling does not appear to have any effect on β_1 receptor-mediated PLB phosphorylation at Serine-16 by cAMP/PKA. Enhanced PI3K signaling does appear to have an anti-adrenergic effect on β_1-induced calcium influx through L-type Ca^{++} channels [147]. The nature of this interaction in the BB- or CCB-toxicity model, as in the present study, is unknown. We assumed that if high-dose insulin impacted upstream events, such as the PI3K pathway or other signaling cascades, it would be reflected in the downstream phosphorylation of PLB.

Our results clearly demonstrate that the mechanism through which HDI exerts its inotropic and lusitropic effects is not mediated by phosphorylation of phospholamban at serine-16 Fig. 23. Similarly, negligible changes in levels of pPLB were detected in isolated, pig SR, subject to other cardiac challenges [149, 150]. There was no serine-16 PLB phosphorylation in any of the HDI-resuscitated pigs, whether made toxic by BBs or CCBs Fig. 23. Despite these negative results in Groups 1-6, cardiac tissue was obtained to compare the effect of a known activator of the β_1-adrenergic receptor, isoproterenol, alone Fig. 21. This result validates the methodology used. PLB phosphorylation was detected, indicating the undetectable P-serine-16 in Groups 1-6 was a valid result (Fig. 21). It is remarkable that no pPLB was detected in any cardiac tissue samples (Fig. 23), except for those treated with isoproterenol (Fig. 21). However, this observation is consistent with the literature, in which quantitative measures of PLB phosphorylation are rare, and the highest reported value for the baseline level is 4% phosphorylation of PLB in ferret myocardia, which increase to 13% upon isoproterenol administration [120].

3.6 Conclusions

Neither phosphorylation of PLB (at serine-16) nor change in total PLB content is the mechanism by which high-dose insulin exerts its inotropic and lusitropic effects, in CCB- and BB-induced cardiovascular toxicity. Thus, it is unlikely that these resuscitative effects are mediated by the cAMP/PKA pathway, either directly or indirectly, through cross-talk with the PI3K pathway.

Chapter 4: Accurate Quantitation of Phospholamban Phosphorylation by Immunoblot

4.1 Summary

We have developed a quantitative immunoblot method to measure the mole fraction of phospholamban (PLB) phosphorylated at Ser16 (X_p) in biological samples. In cardiomyocytes, PLB phosphorylation activates the sarcoplasmic reticulum calcium ATP-ase (SERCA), which reduces cytosolic Ca^{++} to relax the heart during diastole. Unphosphorylated PLB (uPLB) inhibits SERCA at low [Ca^{++}] and phosphorylated PLB (pPLB) is less inhibitory, so myocardial physiology and pathology depend critically on X_p. Current methods of X_p determination by immunoblot provide moderate precision but poor accuracy. We have solved this problem using purified uPLB and pPLB standards, produced by solid-phase peptide synthesis. In each assay, a pair of blots is performed with identical standards and unknowns, using antibodies partially selective for uPLB and pPLB, respectively. When performed on mixtures of uPLB and pPLB, the assay measures both total PLB (tPLB) and X_p with accuracy of 96% or better. We assayed pig cardiac SR and found that X_p varied widely among four animals, from 0.08 to 0.38, but there was remarkably little variation in X_p/tPLB and uPLB/SERCA, suggesting that PLB phosphorylation is tuned to maintain homeostasis in SERCA regulation.

Keywords: Phospholamban, phosphorylation, SERCA, heart failure, western blot, X_p

4.2 Introduction

Phospholamban Phosphorylation and Heart Disease

Heart disease is the number one cause of mortality in the United States across all demographics, and the incidence is rising [4]. In cardiac sarcoplasmic reticulum (CSR), phospholamban (PLB) phosphorylation acts as a molecular switch that activates SERCA (SR Ca-ATP-ase). Active SERCA increases the calcium gradient across the SR during diastole [6], accelerating relaxation and leading to a more forceful systolic contraction [11]. In the presence of unphosphorylated PLB, SERCA is inhibited at submicromolar Ca^{++}, but beta adrenergic phosphorylation of PLB relieves this inhibition [163-166]. Because SERCA activity is reduced in many instances of heart failure [148, 167, 168], SERCA activation is a widely pursued goal for development of new therapies [108]. SERCA inhibition can be relieved by PLB phosphorylation, either at S16 by β-adrenergic activation of PKA [164, 169-171] or at T17 by CaMKII [164], but S16 phosphorylation is more important physiologically [54, 114, 120, 150]. In heart failure, phosphorylation of PLB may be reduced [168, 172], thus it is desirable to increase the fraction of PLB that is phosphorylated (X_p) so that SERCA remains in its active state. PLB phosphorylation at S16 has been examined [6], mimicked [98-100, 173], and altered [55, 174], with the goal of developing therapies for heart failure, but the rational development and testing of these therapies is limited because PLB phosphorylation has not been measured accurately in biological systems. In the present study, we have solved this problem.

Quantitation of X_p in healthy versus failing myocardium is needed to establish correlations between PLB phosphorylation and cardiac function. These correlations will aid in development of prognostic indicators for differential diagnosis and in treatment of heart failure. For example, it has been shown that the R9C mutation in PLB leads to dilated cardiomyopathy [175]. This mutation hinders binding to PKA, thus decreasing phosphorylation [42], but this effect has not been defined in a quantitative measurement of $X_{p,}$ so its role in the disease mechanism remains unclear. Thus X_p measured from biopsied heart tissue (from animal models or patients) would provide crucial insight into the etiology and stages of heart failure, and into the efficacies of therapeutic interventions.

There is one method that has been shown to measure X_p accurately – quantitation of radioactivity after reaction of PLB with γ-^{32}P-ATP in the presence of PKA [123]. However, this method requires an accurate measurement of total PLB (tPLB), and it is limited in

accuracy by the unknown basal phosphorylation state of PLB in most tissue samples. Thus it has usually been used accurately only to analyze simple systems containing purified proteins [32]. It seems clear that a method involving quantitative immunoblots is the method of choice.

Existing Methods Lack Accuracy

However, the properties of PLB have prevented accurate measurement of endogenous X_p by previous immunoblot/densitometry techniques. Phosphorylation of PLB causes only a very slight shift in SDS-PAGE, and this shift is complicated by the multiple oligomeric forms of PLB that are observed [32, 120, 123, 176]. The ideal solution would be a pair of antibodies specific for pPLB and uPLB, respectively. Fortunately, there is a commercially available antibody, designated Ab285, that is almost completely specific for pPLB [122]. Unfortunately, an antibody that is completely specific for uPLB has not been reported. Instead, commercial antibodies that bind uPLB cross-react with pPLB to varying degrees [41, 122, 154, 177]. For example, Ab1d11 [120, 122, 145], AbA1 [178] [179], Ab8A3 [41] [180], and Ab2D12 [177] all bind both uPLB and pPLB, with different degrees of selectivity [177].

As we show below, antibodies that are completely specific for uPLB and pPLB are not strictly required for an accurate assay of X_p. The most important requirement is a source of reliable standards, of known purity and concentration, for both uPLB and pPLB, so that the selectivity of antibodies can be quantitated on immunoblot. Primarily as a result of this lack of reliable standards, previous X_p measurements have not been accurate.

The Present Study

We describe here a quantitative immunoblot method, involving the use of extremely pure synthetic standards for pPLB and uPLB that measures both X_p and tPLB with high accuracy and precision. In our approach, western blots with identical standards and samples were performed, one labeled with Ab285 (almost completely specific for pPLB) and the other with an antibody that is partially selective for uPLB. Following quantitative densitometry of the two immunoblots, a system of simultaneous equations is used to solve accurately for X_p. Using mixtures of standard samples of uPLB and pPLB, the

method is shown to be accurate (less than 5% error), and the method is then used to determine X_p in samples from pig cardiac sarcoplasmic reticulum.

4.3 Methods

PLB Standards

Solid-phase peptide synthesis and HPLC purification were used to prepare porcine uPLB and pPLB standards with > 95% purity, as previously reported [25, 34, 133, 152]. PLB phosphorylation was accomplished by incorporation of p-Ser at position S16 as Fmoc-Ser(PO(OBzl)OH)-OH (EMD Chemicals) during peptide synthesis. Characterization was accomplished by mass spectrometry (MALDI-TOF) and Edman protein sequencing. [25, 34, 133, 152]. PLB concentrations were measured with the BCA assay (Pierce) [6, 25] and by amino acid analysis [25].

Antibodies

Primary antibodies included Ab8A3 [41] [180] (gift from Diana Bigelow, University of Kansas), Ab2D12 [177] (Abcam, Cambridge, MA), AbA1[178] [179] (Millipore, Billerica, MA), and Ab285 [121] (Merck, Westpoint, PA). The first three were monoclonal mouse antibodies. Ab285 is a polyclonal rabbit antibody raised against a cytosolic fragment of pSer16-PLB. Fluorescent dye-conjugated secondary antibodies, used to visualize and quantitate immunoblots, were goat anti-mouse IR-800CW and goat anti-rabbit IR-680LT (LI-COR Biosciences).

Electrophoresis and Western Blot

PLB was dissolved in Laemmli buffer (Biorad) with 5% β-mercaptoethanol, separated by SDS-PAGE on 10-20% Tris-Tricine gels (Biorad) at constant voltage (120 V) for 90 minutes at 25 ^{o}C, and transferred to 0.45 micron Immobilon-FL PVDF membranes (Millipore) in Towbin transfer buffer [153] for 50 minutes at constant current (300 mA), blocked overnight in pure Odyssey blocking buffer (LI-COR Biosciences), and rinsed for 1 minute in ddH_2O. Membranes were then incubated in primary antibody for 1 or 2 hours (at concentrations recommended by the manufacturer) in blocking buffer consisting of 50%

Odyssey blocking buffer and 50% TBS containing 0.1% Tween 20 (TBST). The primary antibody was washed from each blot 3 times for 15 minutes with TBST, before adding secondary antibody at a dilution of 1:15,000 for 35 minutes. The membrane was then washed 3 times for 15 minutes with TBST, and the blots were stored in TBS. Proteins were detected and analyzed using LI-COR Odyssey, using the 700 nm channel for the IR-680LT and the 800 nm channel for the 800CW (LI-COR Biosciences). Analysis by densitometry was accomplished with Odyssey software. The resolution was 169 μm and the focus offset was 0.0 mm. Boxes were drawn around an area that encompassed all PLB bands (monomeric and oligomeric). The background was local, determined as the average or median of the intensities at the top and the bottom of the box. The greatest linearity was obtained at a border width of 1 pixel.

SERCA Quantitation

10 mg of pig CSR was dissolved in 1mL of Laemmli sample buffer (Biorad) containing 4% β-mercaptoethanol, loaded on a 4-20% Tris-HCl gel and electrophoresed at 120V for 90 minutes at 25 ^{o}C. The gel was stained overnight with a solution containing 0.1% coomassie brilliant blue, 40% methanol, 40% H_2O, and 16% acetic acid, and then destained for 1 hour in a solution containing 20% methanol, 5% isopropanol, 10% glacial acetic acid and 65% H_2O. The mass % of SERCA was calculated by densitometry with USCANIT software.

Analysis of Pig Cardiac SR

Pig cardiac SR was prepared from the ventricle of a fresh pig heart, placed on ice within 10 seconds of sacrifice, obtained from Lindenfelser's Meats, Inc (Monticello, MN). One ventricle was dissected and homogenized in a blender with 250 mL of homogenization buffer containing 10 mM $NaHCO_3$, 10 mM Tris-HCl (pH to 7.2 with KOH), 0.8 M Benzamidine, 1mg/L Aprotinin, 1mg/L Leupeptin, 1 M PMSF and 1mg/L pepstatin A. The homogenate was centrifuged at 4˚ C for 20 minutes at 11,000 x g (8,500 rpm in a JA-14). The pellets were discarded and the supernatant was filtered with cheese cloth. The volume of the supernatant was measured, and enough KCl was added to make a 0.6 M KCl solution, which was incubated at 4^{o} C with gentle stirring for

1 hour, then centrifuged at 4 ^{o}C, for 45 minutes at 100,000 x g (36,000 rpm in Beckman 45Ti rotor). The pellet was resuspended using a hand homogenizer, in 15 mL of sucrose buffer (10% sucrose, 20 mM MOPS and 1 mM NaN_3, pH to 7.0 with KOH, 25 g/L aproprotinin, 25 g/L leupeptin, 50 g/L benzamidine, 0.1 M PMSF, and 0.1 g/mL pepstatin A) and centrifuged again for 45 minutes at 100 000 x g. The pellet was resuspended in 1 mL sucrose solution per 40 g of wet weight of tissue with a hand homogenizer. The homogenate was then aliquoted into microfuge tubes (~0.5 mL/tube) flash frozen; and stored at -80 ^{o}C. Electrophoresis and immunoblots were carried out as described above.

Derivation of the Fraction of PLB Phosphorylated

The measured intensity for one band in a western blot using antibody *i* is given by

$$I_i = \Sigma \varepsilon_{ij} c_k \qquad \textbf{Eq. 1 Beer's}$$

ε_{ij} is a proportionality constant (fluorescence units per ng PLB) that describes the slope of the standard curve for uPLB (*j* = *u*) or pPLB (*j* = *p*). The variable c_k is the concentration of uPLB (k = u) or pPLB (k = p) in the unknown sample. As shown below, calculating c_u and c_p requires that one antibody (*i* = *a*) preferentially binds uPLB, and the other antibody (*i* = *b)* preferentially binds pPLB, satisfying the condition $\varepsilon_{au} > \varepsilon_{ap}$ and $\varepsilon_{bu} < \varepsilon_{bp}$). Thus, for our system involving two species (uPLB and pPLB) and two antibodies (*a* partially selective for uPLB and *b* partially selective for pPLB), Eq. 1 expands to

$$I_a = \varepsilon_{au} c_u + \varepsilon_{ap} c_p$$

$$I_b = \varepsilon_{bu} c_u + \varepsilon_{bp} c_p \qquad \textbf{Eq. 2 } \mathbf{I_a}$$

Solve for c_u and c_p:

$$c_u = [I_b \varepsilon_{ap} - I_a \varepsilon_{bp}]/[\varepsilon_{ap}\varepsilon_{bu} - \varepsilon_{au}\varepsilon_{bp}]$$

$$c_p = [I_a \varepsilon_{bu} - I_b \varepsilon_{au}]/[\varepsilon_{ap}\varepsilon_{bu} - \varepsilon_{au}\varepsilon_{bp}] \qquad \textbf{Eq. 3 } \mathbf{c_{Pboth}}$$

Calculate tPLB and X_p:

$$\text{tPLB} = c_p + c_u$$

$$X_p = c_p/\text{tPLB} \qquad \textbf{Eq. 4 } \boldsymbol{X_{pboth}}$$

Statistical Analysis

Statistical analysis was performed using Origin 8.1. For validation of the method, the accuracies of X_p and tPLB values, performed on known mixtures of standards, were calculated as X_p(app)/X_p and tPLB(app)/tPLB, so that 100% accuracy is given by a ratio of 1.00. Precision is expressed as the coefficient of variation (CV = standard deviation/mean). For analysis of true unknowns (pig CSR), values are reported as mean $\pm$ SEM, and one-way ANOVA was used to compare mean values, with a P-value of < 0.01 considered significant. Exact values are reported for $P \geq 0.01$. Slope correlation coefficients (from linear regression) are expressed as Pearson's *r*.

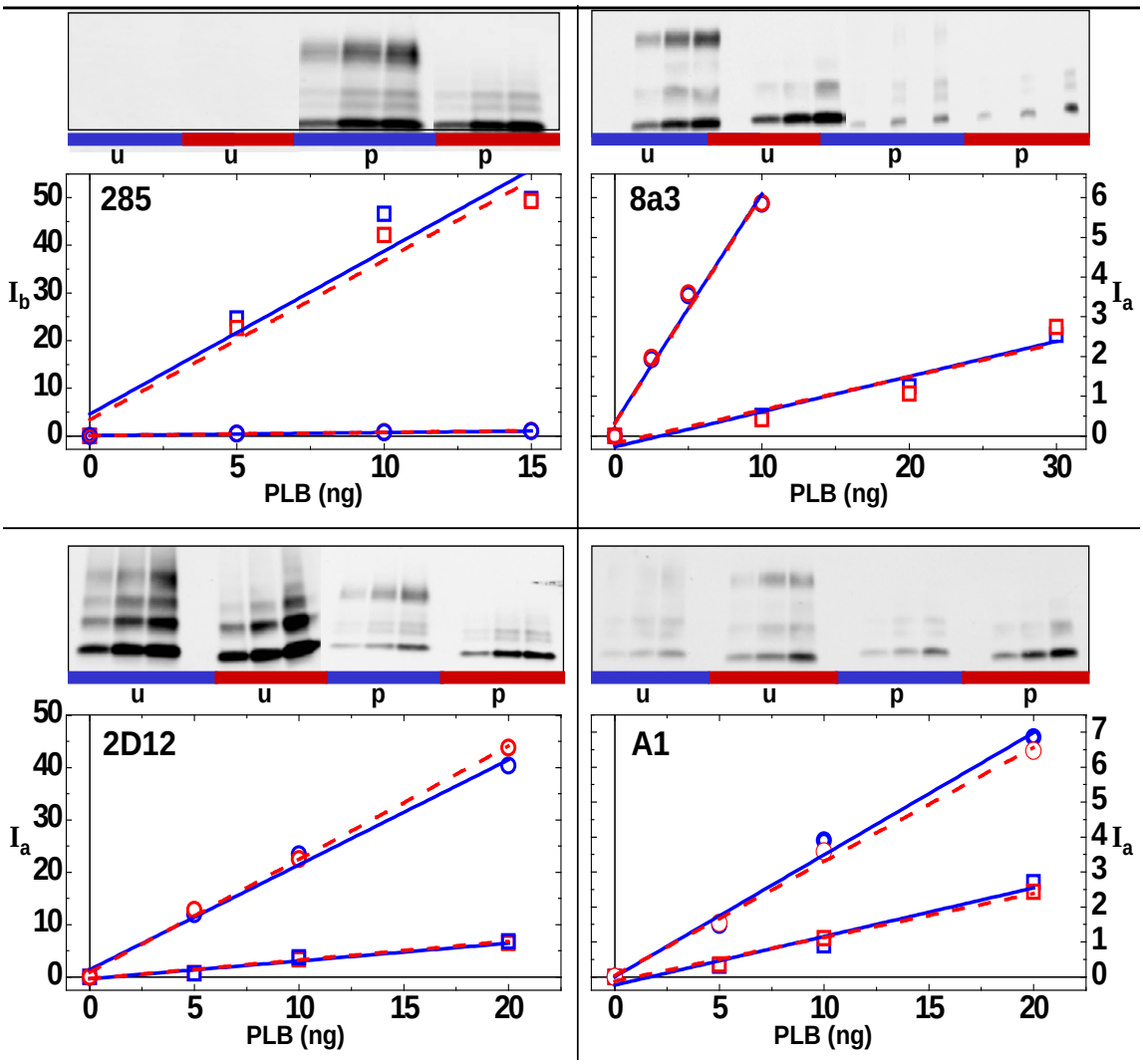

Fig. 24. PLB oligomeric state does not affect immunoblot intensity.
Typical immunoblots and standard curves are shown for samples pre-heated to 100^{o} (red) and unheated (blue) for uPLB ("u" on blots, circles on graphs) or pPLB ("p" on blots, squares on graphs) are shown for Ab285, Ab8A3, Ab2D12, and AbA1. Corresponding western blots are above each graph.

4.4 Results

Densitometry for Oligomeric Forms of PLB

PLB has been shown to exist as a mixture of monomers and oligomers (mainly pentamers), in both native lipid bilayers and on SDS-gels [32, 120, 121, 134, 181], and oligomerization is enhanced by phosphorylation [32, 134]. Therefore, it is essential to determine the effect of the PLB oligomeric state on quantitation by western blot, since it is entirely possible that an antibody would bind less effectively to the five protomers in a PLB pentamer than to the isolated monomer. Fortunately, it has been shown that heating PLB samples to 100^{o}C in SDS solution, just before electrophoresis, greatly

decreases the extent of oligomerization observed on the gel [176]. Therefore, PLB standard curves were analyzed by western blot with and without this pre-heating procedure (Fig. 24). Heating substantially decreased the extent of PLB oligomerization, but there was no significant effect on the observed immunoblot intensity from any of the antibodies (Fig. 24), demonstrating clearly that these immunoblot intensity values are independent of PLB's oligomeric state.

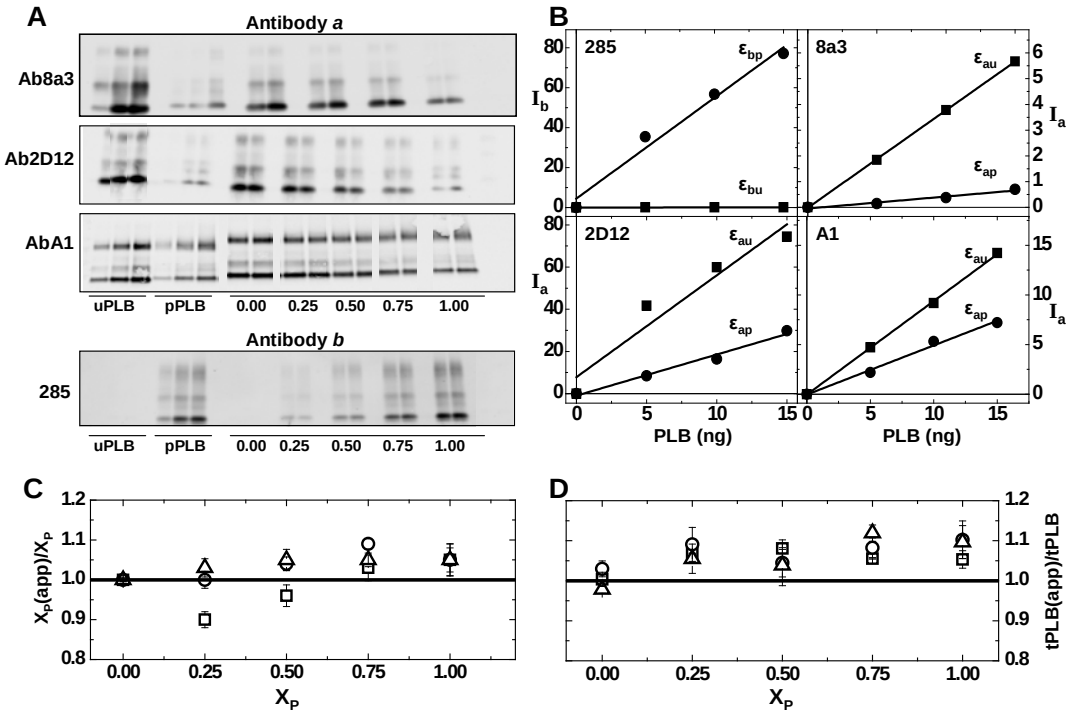

Fig. 25. Validation of the method used to determine X_p and tPLB.
(A) Western blots of 5, 10, and 15 ng of uPLB or pPLB standards, and 12 ng of uPLB/pPLB mixtures (duplicates) of known X_p (0.00 to 1.00, as indicated). (B) Typical standard curves from A for uPLB (squares) and pPLB (circles), from blots incubated with the indicated primary antibody. Resulting slopes (proportionality constants ε_{ij} in Eq. 1 and Eq. 2) are indicated. (C) Accuracy and precision of X_p values: $X_p(app)/X_p$ $\pm$ SEM, for mixtures of known X_p. Antibody *a* is Ab8A3 (square), Ab2D12 (circle), AbA1 (triangle). (D) Accuracy and precision of tPLB values: tPLB(app)/tPLB $\pm$ SEM, for the same mixtures as in C.

Validation of Methodology

Fig. 25 documents the accuracy and precision of our method. Each immunoblot (e.g., Fig. 25A) contains a complete set of synthetic standards (both uPLB and pPLB) and "unknown" mixtures. Fig. 25B shows how the proportionality constants (ε_{ij} in Eq. 1) are determined from standard curves, quantifying each antibody's sensitivity to uPLB and pPLB. For antibody a (Ab8A3, Ab2D12, and AbA1), $\varepsilon_{au} > \varepsilon_{ap}$, confirming that antibody a prefers to bind uPLB over pPLB. Conversely, antibody b (Ab285) greatly prefers to bind pPLB ($\varepsilon_{bu} < \varepsilon_{bp}$) (Fig. 25B). Fig. 25C and Fig. 25D show that the values of X_p and tPLB, determined for the "unknown" mixtures from these blots using Eq. 4, are extremely accurate -- no more than 10% error in all cases. One-way ANOVA showed no significant variation among the mean values for $X_p(app)$ or tPLB, for any of the antibody pairs

This high degree of both accuracy and precision is particularly remarkable in light of the large variability observed for the relative sensitivities of antibodies in separate blots (Table 2). Thus a key requirement of our method is that standards and unknowns are all run on each individual blot a or b, with identical standards and unknowns run on both blots a and b.

Table 1. Accuracy of X_p and tPLB in known mixtures

	Ab8A3	Ab2D12	AbA1	ANOVA
X_p	0.98 ± 0.06	1.04 $\pm$ 0.04	1.05 $\pm$ 0.01	P = 0.98
tPLB	1.10 ± 0.03	1.07 $\pm$ 0.03	1.06 $\pm$ 0.05	P = 0.07

Note: Ab285 was used as the pPLB-selective antibody *b*. The uPLB-selective antibody *a* is given in the top row. Values in columns 2 through 4 indicate accuracy (apparent/actual) $\pm$ precision (coefficient of variation = SD/mean). P > 0.01 indicates no significant variation (n = 8 measurements for each value of X_p for a total of 40).

Table 2. K_{UP}, antibody specificity

Ab	K_{up}		n
	Mean	CV	(blots)
285	0.033	129%	5
8A3	7.47	47%	4
2D12	4.59	36%	4
A1	2.11	26%	4

Note: $K_{UP} = \varepsilon_{iu}/\varepsilon_{ip}$, where i = *a* or *b*. *CV* = coefficient of variation = SD/mean). Primary antibody incubation times were varied from 1 to 2 h.

Potential Sources of Systematic Error

Lack of uPLB and pPLB standards and assumptions made about antibodies create systematic errors in tPLB and X_p measurements. Without standards, accurate measurements cannot be made. When standards are used, Eq. 4 must be used to achieve accuracy, without simplifying assumptions. For example, if it is assumed that antibody *a* reacts equally with uPLB and pPLB ($\varepsilon_{au} = \varepsilon_{ap}$) in determination of tPLB, tPLB is underestimated in the presence of any pPLB, which leads to overestimation of X_p (Fig. 26, Method 1). If it is assumed that antibody *a* is completely specific for uPLB ($\varepsilon_{ap} = 0$), tPLB is systematically overestimated and X_p is systematically underestimated (Fig. 26, Method 2). If it is assumed that antibody b (Ab285) is completely specific for pPLB ($\varepsilon_{bu} = 0$), tPLB and X_p are both overestimated (Fig. 26, Method 3). In the current method Fig. 26, Method 4), all ε_{ij} values were quantitatively included in calculations (Eq. 4). Our method returns X_p and tPLB accurately, with all three choices of antibody *a*, while the systematic errors in Methods 1-3 depend on the choice of antibody *a* (Fig. 26), due to different values of K_{UP} (Table 2).

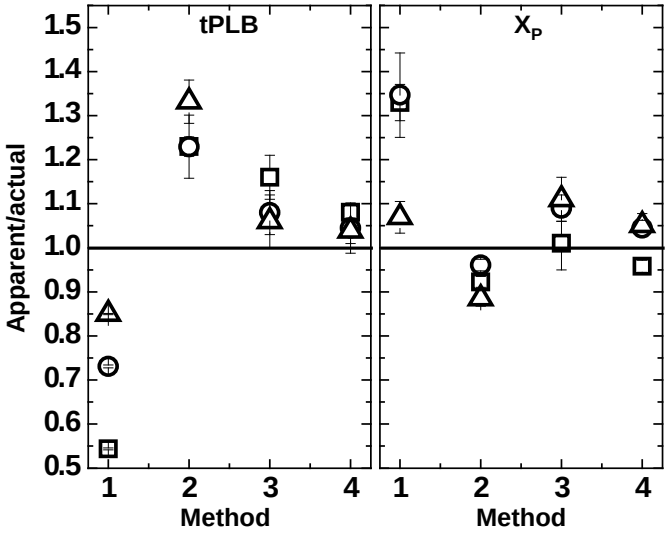

Fig. 26. Comparison of methods for measuring X_p and tPLB for the same sample.
(X_p = 0.5). The line at 1.00 indicates the accurate value. The antibody *a* (partially selective for uPLB) was Ab8A3 (squares), Ab2D12 (circles), or AbA1 (triangles). Methods 1 through 4 and their assumptions are described in the text. Only Method 4 (ours) returns accurate values for both tPLB and X_p.

Application to Pig Cardiac Sarcoplasmic Reticulum (CSR)

X_p and tPLB were measured in cardiac sarcoplasmic reticulum prepared from 4 different pigs (Fig. 27). Standard curves were used to calculate proportionality constants ε_{ij}, and Eq. 4 was used to solve for X_p and tPLB. Mixtures of synthetic standards were used as controls ("X_p control"), yielding accurate values for X_p and tPLB (data not shown), verifying the results of Fig. 25. X_p values were determined with high precision (SEM ≤ .01 for all four pig samples), but there was considerable variation among the four pigs, ranging from 0.08 ± 0.01 to 0.38 ± 0.01 (Fig. 27, Table 3). Similarly, tPLB values were determined with high precision, but varied widely among the four pigs, from 3.32 ± 0.01 nmol/mg to 13.0 ± 1.1 nmol/mg (**Table 3**). Concordantly, ANOVA showed that X_p and tPLB both showed statistically significant variation among the four pigs (Table 3). However, a striking linear correlation between X_p and tPLB was observed (Pearson's r = 0.99), such that CSR containing higher levels of tPLB also have a higher X_p (Fig. 27B, Table 3).

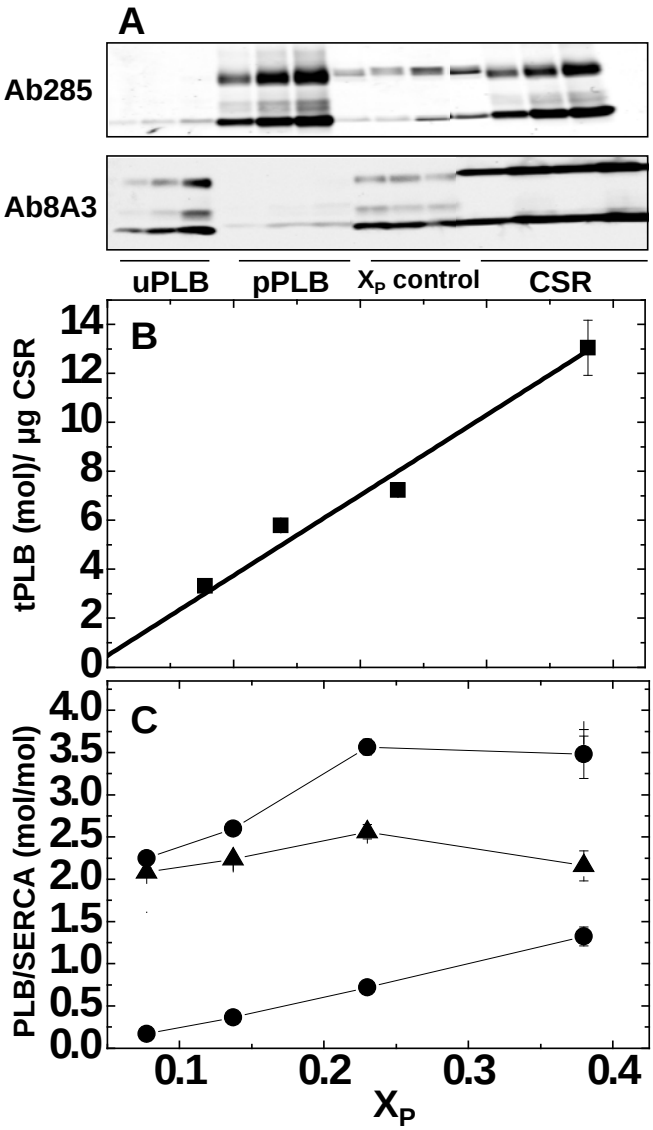

Fig. 27. Application to pig cardiac SR.
(A) Western blots of standards (2.5, 7.5 and 15ng), control mixtures (X_p = 0.25, 0.5 and 0.75), and 0.5µg of pig CSR from pigs 1-4 from left to right. (B) tPLB vs. X_p (C) PLB/SERCA ratios vs. X_p for uPLB, pPLB, and tPLB.

We quantitated the SERCA content in the pig CSR samples using coomassie stain (data not shown). We thus obtained the molar concentrations of SERCA, as well as those of tPLB, uPLB, and pPLB in the four CSR samples. Combining these measurements, we determined the molar ratios of tPLB/SERCA, uPLB/SERCA, and

pPLB/SERCA (Table 3, Fig. 27C). For all four samples, the tPLB/SERCA ratio was consistently greater than 2 (as reported previously in rabbits and rats [180], and uPLB/SERCA was consistently greater than pPLB/SERCA. Both tPLB/SERCA and pPLB/SERCA showed statistically significant variation among the pigs ($P < 0.01$), but it is remarkable that uPLB/SERCA was essentially constant, showing no significant variation among the four pigs ($P = 0.230$) (Table 3**,** Fig. 27C). The Ca-dependence of SERCA enzymatic activity was also found to be essentially invariant among the four pigs (Table 3).

Table 3 Application to pig CSR

	Pig 1	*Pig 2*	*Pig 3*	*Pig 4*	*Mean*	*ANOVA*
X_p	0.08 ± 0.01	0.14 ± 0.01	0.23 ± 0.01	0.38 ± 0.01	0.21 ± 0.03	P < 0.01
tPLB (nmol/mg)	3.32 ± 0.01	5.79 ± 0.10	6.70 ± 0.20	13.0 ± 1.1	7.34 ± 1.03	P < 0.01
uPLB (nmol/mg)	3.07 ± 0.08	4.98 ± 0.08	5.18 ± 0.18	8.09 ± 0.69	5.48 ± 0.52	P < 0.01
pPLB (nmol/mg)	0.25 ± 0.01	0.80 ± 0.03	1.52 ± 0.04	4.96 ± 0.43	1.84 ± 0.53	P < 0.01
SERCA (nmol/mg)	1.48 ± 0.01	2.22 ± 0.01	2.03 ± 0.01	3.74 ± 0.04	2.37 ± 0.24	P < 0.01
pPLB / SERCA (mol/mol)	0.17 ± 0.01	0.36 ± 0.01	0.75 ± 0.02	1.32 ± 0.11	0.65 ± 0.13	P < 0.01
tPLB / SERCA (mol/mol)	2.25 ± 0.05	2.60 ± 0.04	3.31 ± 0.09	3.48 ± 0.14	2.91 ± 0.14	P < 0.01
uPLB / SERCA (mol/mol)	2.08 ± 0.05	2.24 ± 0.03	2.56 ± 0.09	2.16 ± 0.18	2.26 ± 0.05	P = 0.230
pK_{Ca}	5.90 ± 0.01	5.88 ± 0.04	5.87 ± 0.06	5.89 ± 0.01	5.88 + 0.01	P = 0.97

Values are mean ± SEM. $P < 0.01$ indicates significant variation among the four pigs. pK_{Ca} is the pCa value giving half-maximal Ca-ATP-ase activity. n = 5 measurements per pig for all values except pK_{Ca}, where n = 2.

4.5 Discussion

We have established an immunoblot method for the measurement of X_p (the fraction of PLB that is phosphorylated at S16) and tPLB (the total PLB level). This method is extremely accurate (> 96% for X_p, > 90% for tPLB, as shown in Fig. 25 and Table 1

The key to the accuracy of this method is the use of purified synthetic standards of uPLB and pPLB, along with antibodies that are partially selective for each, and rigorous calculations (Eq. 4). Without these features, substantial systematic errors result (Fig. 26).

When the method was applied to pig CSR obtained from different animals (Fig. 27), the X_p values were observed to be quite variable, ranging from 0.08 to 0.38 for four animals. Values of tPLB also varied widely, but there was a remarkably precise linear correlation between tPLB and X_p (Fig. 27B). We also measured SERCA content and used it to calculate PLB/SERCA ratios. While pPLB/SERCA and tPLB/SERCA varied widely, there were no significant variations in uPLB/SERCA among the four pigs (Fig. 27, Table 3). The regulation of SERCA by PLB, as indicated by Ca dependence of ATP-ase activity, was also invariant among the four pigs (Table 3, pK_{Ca}).

Features of Our Method

The key features of our method are calibration within each immunoblot and a rigorously accurate calculation of X_p and tPLB with Eq. 4, which combines two immunoblots. Calibration requires that both uPLB and pPLB standards of known concentration and phosphorylation state are available to generate standard curves and determine a unique set of proportionality constants for each blot. Due to variability of K_{UP} among immunoblots (Table 2), standards and samples must be run on the same blot. In order to use Eq. 4 to calculate X_p and tPLB reliably, the two blots (*a* and *b*), must have identical standards and unknowns, and blots *a* and *b* must be incubated with two antibodies with opposite selectivity for uPLB and pPLB. If any of these features are missing, differences in antibody selectivity and sensitivity of isolated experiments introduce systematic errors into X_p(app) and tPLB(app) calculations Fig. 26. Indeed, most measurements of PLB phosphorylation have lacked standards for uPLB and pPLB, so measurements were relative, inherently lacking accuracy [94, 113, 114, 116, 117, 119]. For example, a sample that has 4 times more phosphorylation than a control may represent an increase from 0.03 to 0.12 (probably having little physiological effect) [120] [155]or from 0.25 to 1.00 (probably having a substantial physiological effect) [119]. There is only one paper in the literature in which standards of both uPLB and pPLB were used, along with a pair of antibodies with differential sensitivity, but that study did not attempt quantitative calculations such as those in Eq. 4 [154]. Even with standards, Fig. 26

illustrates how assumptions about antibody selectivity can lead to systematic errors in determination of both tPLB and X_p.

This study focused on PLB phosphorylation at S16 because that site is more important physiologically than T17 [114], due mainly to the lower level of phosphorylation at T17 [120]. Phosphorylation of PLB at T17 must be potentiated by S16 phosphorylation ([182]), and T17 phosphorylation has negligible effect after S16 has been phosphorylated [123]. Nevertheless, this method has the capacity to measure PLB phosphorylation at T17, using an antibody that is selective for T17-pPLB (commercially available from Santa Cruz Biotechnology, Inc. CA, USA, or Badrilla Ltd, Leeds, UK,), and threonine-17-phosphorylated pPLB synthetic standard.

Application to Biological Membranes

We have used our method to make the first accurate measurements of X_p and tPLB in biological samples. We found that the fraction of phosphorylated phospholamban (X_p) in pig CSR is variable, ranging from 0.08 $\pm$ 0.01 to 0.38 $\pm$ 0.03 (Table 3). Note that even the greatest X_p value was less than 0.5, leaving considerable reserve for response to β-adrenergic stimulation or response to phosphomimetic therapies [183]. The total PLB level, tPLB, was also quite variable, ranging from (3.32 $\pm$ 0.05 nmol/mg total protein) to (13.0 $\pm$ 1.13 nmol/mg total protein) (Table 3). Despite the wide variation in X_p and tPLB among the pigs, the ratio of X_p to tPLB was essentially constant (Fig. 27B), suggesting that PLB phosphorylation increases in order to compensate for the inhibitory effects of high PLB expression. To further explore this hypothesis, we measured SERCA content in the same pig CSR samples, then calculated molar ratios tPLB/SERCA, uPLB/SERCA and pPLB/SERCA (Table 3). Differences in tPLB/SERCA, pPLB/SERCA and X_p were all statistically significant among the four pigs ($P < 0.01$), as was the difference in SERCA content ($P < 0.01$), but uPLB/SERCA did not vary significantly among the four pigs, over a wide range of X_p and SERCA measurements (Fig. 27C, Table 3). Similarly, the Ca-dependence of SERCA ATP-ase activity was essentially invariant (Table 3). These results suggest that myocytes in non-failing myocardium maintain SERCA activity by keeping uPLB/SERCA within a narrow range. Future studies are needed to test this hypothesis more rigorously. For example, freshly harvested tissue should be

homogenized and analyzed quickly, using phosphatase inhibitors to ensure that the phosphorylation status of PLB is captured accurately [114].

Potential Applications to Research in Physiology and Pathology

Now that we can quantitate c_u, c_p, X_p, tPLB, and SERCA with accuracy and precision, many questions concerning the role of PLB in cardiac function and pathology can be addressed more quantitatively to evaluate their roles in cardiovascular physiology and pathology. This method should standardize X_p and tPLB measurements across studies, even if the blots are performed in different laboratories, where the choice of primary antibodies and other experimental conditions may vary. The accuracy of our method should normalize X_p and tPLB values across animal systems, sample preparations, disease states, and therapies so that cross-study comparisons can be made. With this method in hand, it is possible to test the hypothesis that the uPLB/SERCA ratio increases in heart failure, resulting in decreased SERCA activity (increased pK_{Ca}) [123]. Thus significant increases in uPLB/SERCA ratio may be a useful biomarker for heart disease and/or response to therapy in animal models of heart failure. The variation in X_p and tPLB (Fig. 27) suggests that it is uPLB/SERCA that should be measured in these models, providing reference values for comparisons during diagnosis and over the course of treatment.

Potential Clinical Applications

Our method has potential for clinical applications to assess changes in X_p in human cardiac tissue, in response to current treatments such as β-adrenergic agonists, Ca^{++} channel blockers, phosphodiesterases, and future treatments in gene and drug therapy. Since milligram quantities of tissue are sufficient for replicate measurements of X_p, tPLB and uPLB/SERCA, it is plausible that human biopsies (1-2 mm^3 of tissue) [184], which are performed routinely under suspicion of myocarditis, cardiomyopathy and amyloidosis, can also be assayed for these values. Myocardial biopsy is a non-surgical procedure with a complication rate of <1% to the patient [184]. Accurate tPLB calculations can also quantitatively determine changes in PLB expression, revealing

factors that affect calcium regulation at the level of transcription or translation. Thus our method can play an important role in evaluating the success of gene or drug therapies for heart failure. More generally, our approach can provide a quantitative measure of any post-translational modification where (a) purified standards are available for both the unmodified and modified state of the protein and (b) antibodies are available with differential sensitivity to the posttranslational modification.

Bibliography

1. Minino, A.M., *Death in the United States, 2009.* NCHS Data Brief, (64): p. 1-8.
2. Roger, V.L., et al., *Heart disease and stroke statistics--2011 update: a report from the American Heart Association.* Circulation. **123**(4): p. e18-e209.
3. Lloyd-Jones, D., et al., *Heart disease and stroke statistics--2010 update: a report from the American Heart Association.* Circulation. **121**(7): p. e46-e215.
4. Heron, M., et al., *Deaths: final data for 2006.* Natl Vital Stat Rep, 2009. **57**(14): p. 1-134.
5. Abelev, B., et al., *Production of Muons from Heavy Flavor Decays at Forward Rapidity in pp and Pb-Pb Collisions at sqrt[s_{NN}]=2.76 TeV.* Phys Rev Lett, 2012. **109**(11): p. 112301.
6. Karim, C.B., et al., *Phosphorylation-dependent Conformational Switch in Spin-labeled Phospholamban Bound to SERCA.* J Mol Biol, 2006. **358**(4): p. 1032-40.
7. Kimura, Y., et al., *Phospholamban regulates the Ca2+-ATPase through intramembrane interactions.* J Biol Chem, 1996. **271**(36): p. 21726-31.
8. Villars, P.S., et al., *Role of diastole in left ventricular function, I: Biochemical and biomechanical events.* Am J Crit Care, 2004. **13**(5): p. 394-403; quiz 404-5.
9. Lipskaia, L., et al., *Sarcoplasmic reticulum Ca(2+) ATPase as a therapeutic target for heart failure.* Expert Opin Biol Ther. **10**(1): p. 29-41.
10. Periasamy, M. and S. Huke, *SERCA pump level is a critical determinant of Ca(2+)homeostasis and cardiac contractility.* J Mol Cell Cardiol, 2001. **33**(6): p. 1053-63.
11. Bers, D.M., *Cardiac excitation-contraction coupling.* Nature, 2002. **415**(6868): p. 198-205.
12. N. Thompson, M.T. *Anatomy of the heart*. 2010 [cited 2012 10/09/12]; Available from: http://www.bami.us/CardiacAnatomy.html.
13. Costanzo, L.S., *Physiology*, ed. L.W. Wilkins. 2007.
14. Lilly, L.S., *Pathophysiology of Heart Disease*. Third ed, ed. L.S. Lilly. 2003, Philadelphia: Lippincott and Wilkins. 445.
15. Zucchi, R. and S. Ronca-Testoni, *The sarcoplasmic reticulum Ca2+ channel/ryanodine receptor: modulation by endogenous effectors, drugs and disease states.* Pharmacol Rev, 1997. **49**(1): p. 1-51.
16. Starling, E.a.V., MB, *The regulation of the energy of output of he thuman heart.* J Physiol, 1926. **62**: p. 243-261.
17. Li, L., et al., *Phosphorylation of phospholamban and troponin I in beta-adrenergic-induced acceleration of cardiac relaxation.* Am J Physiol Heart Circ Physiol, 2000. **278**(3): p. H769-79.
18. Dostal, D.E. and L.E. Watson, *Understanding diastolic heart failure with preserved ejection fraction: choosing the right model.* Hypertension, 2006. **47**(5): p. 830-2.
19. Mandinov, L., et al., *Diastolic heart failure.* Cardiovasc Res, 2000. **45**(4): p. 813-25.

20. Wang, Y., et al., *Astragalosides rescue both cardiac function and sarcoplasmic reticulum Ca(2)(+) transport in rats with chronic heart failure.* Phytother Res. **26**(2): p. 231-8.
21. Dieterle, T., et al., *Gene transfer of a phospholamban-targeted antibody improves calcium handling and cardiac function in heart failure.* Cardiovasc Res, 2005. **67**(4): p. 678-88.
22. Janczewski, A.M., et al., *Phospholamban gene ablation improves calcium transients but not cardiac function in a heart failure model.* Cardiovasc Res, 2004. **62**(3): p. 468-80.
23. Minamisawa, S., et al., *Chronic phospholamban-sarcoplasmic reticulum calcium ATPase interaction is the critical calcium cycling defect in dilated cardiomyopathy.* Cell, 1999. **99**(3): p. 313-22.
24. Mueller, B., et al., *Direct detection of phospholamban and sarcoplasmic reticulum Ca-ATPase interaction in membranes using fluorescence resonance energy transfer.* Biochemistry, 2004. **43**(27): p. 8754-65.
25. Karim, C.B., et al., *Phospholamban structural dynamics in lipid bilayers probed by a spin label rigidly coupled to the peptide backbone.* Proc Natl Acad Sci U S A, 2004. **101**(40): p. 14437-42.
26. Traaseth, N.J., et al., *Spectroscopic validation of the pentameric structure of phospholamban.* Proc Natl Acad Sci U S A, 2007. **104**(37): p. 14676-81.
27. Traaseth, N.J., et al., *Structural dynamics and topology of phospholamban in oriented lipid bilayers using multidimensional solid-state NMR.* Biochemistry, 2006. **45**(46): p. 13827-34.
28. Zamoon, J., et al., *NMR solution structure and topological orientation of monomeric phospholamban in dodecylphosphocholine micelles.* Biophys J, 2003. **85**(4): p. 2589-98.
29. Traaseth, N.J., et al., *Structure and topology of monomeric phospholamban in lipid membranes determined by a hybrid solution and solid-state NMR approach.* Proc Natl Acad Sci U S A, 2009. **106**(25): p. 10165-70.
30. Manna, M. and C. Mukhopadhyay, *Cholesterol driven alteration of the conformation and dynamics of phospholamban in model membranes.* Phys Chem Chem Phys. **13**(45): p. 20188-98.
31. Reddy, L.G., L.R. Jones, and D.D. Thomas, *Depolymerization of phospholamban in the presence of calcium pump: a fluorescence energy transfer study.* Biochemistry, 1999. **38**(13): p. 3954-62.
32. Cornea, R.L., et al., *Mutation and phosphorylation change the oligomeric structure of phospholamban in lipid bilayers.* Biochemistry, 1997. **36**(10): p. 2960-7.
33. Cornea, R.L., et al., *Reexamination of the role of the leucine/isoleucine zipper residues of phospholamban in inhibition of the Ca2+ pump of cardiac sarcoplasmic reticulum.* J Biol Chem, 2000. **275**(52): p. 41487-94.
34. Karim, C.B., et al., *Synthetic null-cysteine phospholamban analogue and the corresponding transmembrane domain inhibit the Ca-ATPase.* Biochemistry, 2000. **39**(35): p. 10892-7.

35. Li, J., *Probing Cardiac Calcium Regulation Using Time-Resolved Optical Spectroscopy*, in *Physics*. 2012, University of Minnesota: Minneapolis.
36. Fujii, J., et al., *Complete complementary DNA-derived amino acid sequence of canine cardiac phospholamban.* J Clin Invest, 1987. **79**(1): p. 301-4.
37. Metcalfe, E.E., et al., *(1)H/(15)N heteronuclear NMR spectroscopy shows four dynamic domains for phospholamban reconstituted in dodecylphosphocholine micelles.* Biophys J, 2004. **87**(2): p. 1205-14.
38. Tatulian, S.A., et al., *Secondary structure and orientation of phospholamban reconstituted in supported bilayers from polarized attenuated total reflection FTIR spectroscopy.* Biochemistry, 1995. **34**(13): p. 4448-56.
39. Arkin, I.T., et al., *Structural model of the phospholamban ion channel complex in phospholipid membranes.* J Mol Biol, 1995. **248**(4): p. 824-34.
40. Oxenoid, K. and J.J. Chou, *The structure of phospholamban pentamer reveals a channel-like architecture in membranes.* Proc Natl Acad Sci U S A, 2005. **102**(31): p. 10870-5.
41. Robia, S.L., N.C. Flohr, and D.D. Thomas, *Phospholamban pentamer quaternary conformation determined by in-gel fluorescence anisotropy.* Biochemistry, 2005. **44**(11): p. 4302-11.
42. Ha, K.N., et al., *Lethal Arg9Cys phospholamban mutation hinders Ca2+-ATPase regulation and phosphorylation by protein kinase A.* Proc Natl Acad Sci U S A. **108**(7): p. 2735-40.
43. Simmerman, H.K., et al., *Sequence analysis of phospholamban. Identification of phosphorylation sites and two major structural domains.* J Biol Chem, 1986. **261**(28): p. 13333-41.
44. Mundina-Weilenmann, C., et al., *Immunodetection of phosphorylation sites gives new insights into the mechanisms underlying phospholamban phosphorylation in the intact heart.* J Biol Chem, 1996. **271**(52): p. 33561-7.
45. Masterson, L.R., et al., *cAMP-dependent protein kinase A selects the excited state of the membrane substrate phospholamban.* J Mol Biol, 2011. **412**(2): p. 155-64.
46. Colyer, J., *Phosphorylation states of phospholamban.* Ann N Y Acad Sci, 1998. **853**: p. 79-91.
47. Mattiazzi, A. and E.G. Kranias, *CaMKII regulation of phospholamban and SR Ca2+ load.* Heart Rhythm. **8**(5): p. 784-7.
48. Bartel, S., et al., *Phosphorylation of phospholamban at threonine-17 in the absence and presence of beta-adrenergic stimulation in neonatal rat cardiomyocytes.* J Mol Cell Cardiol, 2000. **32**(12): p. 2173-85.
49. Dash, R., et al., *Gender influences on sarcoplasmic reticulum Ca2+-handling in failing human myocardium.* J Mol Cell Cardiol, 2001. **33**(7): p. 1345-53.
50. Mills, G.D., et al., *Phosphorylation of phospholamban at threonine-17 reduces cardiac adrenergic contractile responsiveness in chronic pressure overload-induced hypertrophy.* Am J Physiol Heart Circ Physiol, 2006. **291**(1): p. H61-70.
51. Vittone, L., C. Mundina-Weilenmann, and A. Mattiazzi, *Phospholamban phosphorylation by CaMKII under pathophysiological conditions.* Front Biosci, 2008. **13**: p. 5988-6005.

52. Grimm, M. and J.H. Brown, *Beta-adrenergic receptor signaling in the heart: role of CaMKII.* J Mol Cell Cardiol, 2010. **48**(2): p. 322-30.
53. Wang, W., et al., *Sustained beta1-adrenergic stimulation modulates cardiac contractility by Ca2+/calmodulin kinase signaling pathway.* Circ Res, 2004. **95**(8): p. 798-806.
54. Mattiazzi, A., et al., *Role of phospholamban phosphorylation on Thr17 in cardiac physiological and pathological conditions.* Cardiovasc Res, 2005. **68**(3): p. 366-75.
55. Nicolaou, P., R.J. Hajjar, and E.G. Kranias, *Role of protein phosphatase-1 inhibitor-1 in cardiac physiology and pathophysiology.* J Mol Cell Cardiol, 2009. **47**(3): p. 365-71.
56. Foulkes, J.G., et al., *A kinetic analysis of the effects of inhibitor-1 and inhibitor-2 on the activity of protein phosphatase-1.* Eur J Biochem, 1983. **132**(2): p. 309-13.
57. Huang, F.L. and W.H. Glinsmann, *Separation and characterization of two phosphorylase phosphatase inhibitors from rabbit skeletal muscle.* Eur J Biochem, 1976. **70**(2): p. 419-26.
58. Nicolaou, P. and E.G. Kranias, *Role of PP1 in the regulation of Ca cycling in cardiac physiology and pathophysiology.* Front Biosci, 2009. **14**: p. 3571-85.
59. Paterlini, M.G. and D.D. Thomas, *The alpha-helical propensity of the cytoplasmic domain of phospholamban: a molecular dynamics simulation of the effect of phosphorylation and mutation.* Biophys J, 2005. **88**(5): p. 3243-51.
60. Quirk, P.G., et al., *Conformational effects of serine phosphorylation in phospholamban peptides.* Eur J Biochem, 1996. **236**(1): p. 85-91.
61. Mortishire-Smith, R.J., et al., *Solution structure of the cytoplasmic domain of phopholamban: phosphorylation leads to a local perturbation in secondary structure.* Biochemistry, 1995. **34**(23): p. 7603-13.
62. Metcalfe, E.E., N.J. Traaseth, and G. Veglia, *Serine 16 phosphorylation induces an order-to-disorder transition in monomeric phospholamban.* Biochemistry, 2005. **44**(11): p. 4386-96.
63. Traaseth, N.J., D.D. Thomas, and G. Veglia, *Effects of Ser16 phosphorylation on the allosteric transitions of phospholamban/Ca(2+)-ATPase complex.* J Mol Biol, 2006. **358**(4): p. 1041-50.
64. Nesmelov, Y.E., et al., *Rotational dynamics of phospholamban determined by multifrequency electron paramagnetic resonance.* Biophys J, 2007. **93**(8): p. 2805-12.
65. Li, J., et al., *Structural and functional dynamics of an integral membrane protein complex modulated by lipid headgroup charge.* J Mol Biol. **418**(5): p. 379-89.
66. Fairclough, R.J., et al., *Effect of Hailey-Hailey Disease mutations on the function of a new variant of human secretory pathway Ca2+/Mn2+-ATPase (hSPCA1).* J Biol Chem, 2003. **278**(27): p. 24721-30.
67. Toyoshima, C., et al., *Crystal structure of the calcium pump of sarcoplasmic reticulum at 2.6 A resolution.* Nature, 2000. **405**(6787): p. 647-55.
68. Moller, J.V., et al., *The sarcoplasmic Ca2+-ATPase: design of a perfect chemi-osmotic pump.* Q Rev Biophys. **43**(4): p. 501-66.

69. Brini, M. and E. Carafoli, *Calcium pumps in health and disease.* Physiol Rev, 2009. **89**(4): p. 1341-78.
70. Wuytack, F., L. Raeymaekers, and L. Missiaen, *Molecular physiology of the SERCA and SPCA pumps.* Cell Calcium, 2002. **32**(5-6): p. 279-305.
71. De Meis, L. and W. Hasselbach, *Acetyl phosphate as substrate for Ca 2+ uptake in skeletal muscle microsomes. Inhibition by alkali ions.* J Biol Chem, 1971. **246**(15): p. 4759-63.
72. Sacchetto, R., et al., *Crystal structure of sarcoplasmic reticulum Ca2+-ATPase (SERCA) from bovine muscle.* J Struct Biol. **178**(1): p. 38-44.
73. Toyoshima, C. and H. Nomura, *Structural changes in the calcium pump accompanying the dissociation of calcium.* Nature, 2002. **418**(6898): p. 605-11.
74. Yu, X., et al., *H+ countertransport and electrogenicity of the sarcoplasmic reticulum Ca2+ pump in reconstituted proteoliposomes.* Biophys J, 1993. **64**(4): p. 1232-42.
75. Dally, S., et al., *Multiple and diverse coexpression, location, and regulation of additional SERCA2 and SERCA3 isoforms in nonfailing and failing human heart.* J Mol Cell Cardiol. **48**(4): p. 633-44.
76. Toyoshima, C., *Structure determination of tubular crystals of membrane proteins. I. Indexing of diffraction patterns.* Ultramicroscopy, 2000. **84**(1-2): p. 1-14.
77. Toyoshima, C., et al., *Modeling of the inhibitory interaction of phospholamban with the Ca2+ ATPase.* Proc Natl Acad Sci U S A, 2003. **100**(2): p. 467-72.
78. MacLennan, D.H., et al., *Amino-acid sequence of a Ca2+ + Mg2+-dependent ATPase from rabbit muscle sarcoplasmic reticulum, deduced from its complementary DNA sequence.* Nature, 1985. **316**(6030): p. 696-700.
79. Brandl, C.J., et al., *Two Ca2+ ATPase genes: homologies and mechanistic implications of deduced amino acid sequences.* Cell, 1986. **44**(4): p. 597-607.
80. Ji, Y., et al., *SERCA1a can functionally substitute for SERCA2a in the heart.* Am J Physiol, 1999. **276**(1 Pt 2): p. H89-97.
81. Lalli, M.J., et al., *Sarcoplasmic reticulum Ca(2+) atpase (SERCA) 1a structurally substitutes for SERCA2a in the cardiac sarcoplasmic reticulum and increases cardiac Ca(2+) handling capacity.* Circ Res, 2001. **89**(2): p. 160-7.
82. Gelebart, P., et al., *Identification of a new SERCA2 splice variant regulated during monocytic differentiation.* Biochem Biophys Res Commun, 2003. **303**(2): p. 676-84.
83. Dally, S., et al., *Ca2+-ATPases in non-failing and failing heart: evidence for a novel cardiac sarco/endoplasmic reticulum Ca2+-ATPase 2 isoform (SERCA2c).* Biochem J, 2006. **395**(2): p. 249-58.
84. Toyofuku, T., et al., *Amino acids Lys-Asp-Asp-Lys-Pro-Val402 in the Ca(2+)-ATPase of cardiac sarcoplasmic reticulum are critical for functional association with phospholamban.* J Biol Chem, 1994. **269**(37): p. 22929-32.
85. Chen, Z., et al., *Cross-linking of C-terminal residues of phospholamban to the Ca2+ pump of cardiac sarcoplasmic reticulum to probe spatial and functional interactions within the transmembrane domain.* J Biol Chem, 2006. **281**(20): p. 14163-72.

86. Hutter, M.C., et al., *A structural model of the complex formed by phospholamban and the calcium pump of sarcoplasmic reticulum obtained by molecular mechanics.* Chembiochem, 2002. **3**(12): p. 1200-8.
87. Cantilina, T., et al., *Comparative studies of cardiac and skeletal sarcoplasmic reticulum ATPases. Effect of a phospholamban antibody on enzyme activation by Ca2+.* J Biol Chem, 1993. **268**(23): p. 17018-25.
88. Glaves, J.P., et al., *Phosphorylation and mutation of phospholamban alter physical interactions with the sarcoplasmic reticulum calcium pump.* J Mol Biol. **405**(3): p. 707-23.
89. Thomas, D.D., et al., *Direct spectroscopic detection of molecular dynamics and interactions of the calcium pump and phospholamban.* Ann N Y Acad Sci, 1998. **853**: p. 186-94.
90. Li, M., et al., *A fluorescence energy transfer method for analyzing protein oligomeric structure: application to phospholamban.* Biophys J, 1999. **76**(5): p. 2587-99.
91. Autry, J.M. and L.R. Jones, *Functional Co-expression of the canine cardiac Ca2+ pump and phospholamban in Spodoptera frugiperda (Sf21) cells reveals new insights on ATPase regulation.* J Biol Chem, 1997. **272**(25): p. 15872-80.
92. Kimura, Y., et al., *Phospholamban inhibitory function is activated by depolymerization.* J Biol Chem, 1997. **272**(24): p. 15061-4.
93. Tada, M. and M. Kadoma, *Regulation of the Ca2+ pump ATPase by cAMP-dependent phosphorylation of phospholamban.* Bioessays, 1989. **10**(5): p. 157-63.
94. Jackson, W.A. and J. Colyer, *Translation of Ser16 and Thr17 phosphorylation of phospholamban into Ca 2+-pump stimulation.* Biochem J, 1996. **316 (Pt 1)**: p. 201-7.
95. Gustavsson, M., et al., *Lipid-mediated folding/unfolding of phospholamban as a regulatory mechanism for the sarcoplasmic reticulum Ca2+-ATPase.* J Mol Biol. **408**(4): p. 755-65.
96. Lockamy, E.L., et al., *Functional and physical competition between phospholamban and its mutants provides insight into the molecular mechanism of gene therapy for heart failure.* Biochem Biophys Res Commun. **408**(3): p. 388-92.
97. Hou, Z., E.M. Kelly, and S.L. Robia, *Phosphomimetic mutations increase phospholamban oligomerization and alter the structure of its regulatory complex.* J Biol Chem, 2008. **283**(43): p. 28996-9003.
98. Oxenoid, K., A.J. Rice, and J.J. Chou, *Comparing the structure and dynamics of phospholamban pentamer in its unphosphorylated and pseudo-phosphorylated states.* Protein Sci, 2007. **16**(9): p. 1977-83.
99. Hoshijima, M., et al., *Chronic suppression of heart-failure progression by a pseudophosphorylated mutant of phospholamban via in vivo cardiac rAAV gene delivery.* Nat Med, 2002. **8**(8): p. 864-71.
100. Ha, K.N., et al., *Controlling the inhibition of the sarcoplasmic Ca2+-ATPase by tuning phospholamban structural dynamics.* J Biol Chem, 2007. **282**(51): p. 37205-14.

101. Ha, K.N., M. Gustavsson, and G. Veglia, *Tuning the structural coupling between the transmembrane and cytoplasmic domains of phospholamban to control sarcoplasmic reticulum Ca(2+)-ATPase (SERCA) function.* J Muscle Res Cell Motil, 2012.
102. Ziolo, M.T., et al., *Adenoviral gene transfer of mutant phospholamban rescues contractile dysfunction in failing rabbit myocytes with relatively preserved SERCA function.* Circ Res, 2005. **96**(8): p. 815-7.
103. Gruber, S.J., S. Haydon, and D.D. Thomas, *Phospholamban mutants compete with wild type for SERCA binding in living cells.* Biochem Biophys Res Commun, 2012. **420**(2): p. 236-40.
104. Zhang, H.S., et al., *A designed zinc-finger transcriptional repressor of phospholamban improves function of the failing heart.* Mol Ther, 2012. **20**(8): p. 1508-15.
105. Haghighi, K., et al., *Human phospholamban null results in lethal dilated cardiomyopathy revealing a critical difference between mouse and human.* J Clin Invest, 2003. **111**(6): p. 869-76.
106. Miyazaki, Y., et al., *Heart failure-inducible gene therapy targeting protein phosphatase 1 prevents progressive left ventricular remodeling.* PLoS One, 2012. **7**(4): p. e35875.
107. Jaski, B.E., et al., *Calcium upregulation by percutaneous administration of gene therapy in cardiac disease (CUPID Trial), a first-in-human phase 1/2 clinical trial.* J Card Fail, 2009. **15**(3): p. 171-81.
108. Jessup, M., et al., *Calcium Upregulation by Percutaneous Administration of Gene Therapy in Cardiac Disease (CUPID): a phase 2 trial of intracoronary gene therapy of sarcoplasmic reticulum Ca2+-ATPase in patients with advanced heart failure.* Circulation, 2011. **124**(3): p. 304-13.
109. Cornea, R.L., et al., *High-Throughput FRET Assay Yields Allosteric SERCA Activators.* J Biomol Screen.
110. Gheorghiade, M., et al., *Hemodynamic, echocardiographic, and neurohormonal effects of istaroxime, a novel intravenous inotropic and lusitropic agent: a randomized controlled trial in patients hospitalized with heart failure.* J Am Coll Cardiol, 2008. **51**(23): p. 2276-85.
111. Kairouz, V., et al., *Molecular targets in heart failure gene therapy: current controversies and translational perspectives.* Ann N Y Acad Sci, 2012. **1254**: p. 42-50.
112. Ablorh, N.A., et al., *Accurate quantitation of phospholamban phosphorylation by immunoblot.* Anal Biochem. **425**(1): p. 68-75.
113. Calaghan, S., L. Kozera, and E. White, *Compartmentalisation of cAMP-dependent signalling by caveolae in the adult cardiac myocyte.* J Mol Cell Cardiol, 2008. **45**(1): p. 88-92.
114. Calaghan, S., E. White, and J. Colyer, *Preservation of the in vivo phosphorylation status of phospholamban in the heart: evidence for a site-specific difference in the dephosphorylation of phospholamban.* Biochem Biophys Res Commun, 1998. **248**(3): p. 701-5.

115. Calaghan, S.C., E. White, and J. Colyer, *Co-ordinated changes in cAMP, phosphorylated phospholamban, Ca2+ and contraction following beta-adrenergic stimulation of rat heart.* Pflugers Arch, 1998. **436**(6): p. 948-56.
116. Grote-Wessels, S., et al., *Inhibition of protein phosphatase 1 by inhibitor-2 exacerbates progression of cardiac failure in a model with pressure overload.* Cardiovasc Res, 2008. **79**(3): p. 464-71.
117. Guinto, P.J., et al., *Temporal and mutation-specific alterations in Ca2+ homeostasis differentially determine the progression of cTnT-related cardiomyopathies in murine models.* Am J Physiol Heart Circ Physiol, 2009. **297**(2): p. H614-26.
118. Jackson, T., et al., *FDG PET/CT interobserver agreement in head and neck cancer: FDG and CT measurements of the primary tumor site.* Nucl Med Commun, 2012. **33**(3): p. 305-12.
119. Loyer, X., et al., *Cardiomyocyte overexpression of neuronal nitric oxide synthase delays transition toward heart failure in response to pressure overload by preserving calcium cycling.* Circulation, 2008. **117**(25): p. 3187-98.
120. Mayer, E.J., et al., *Characterization and quantitation of phospholamban and its phosphorylation state using antibodies.* Biochem Biophys Res Commun, 2000. **267**(1): p. 40-8.
121. Mayer, E.J., et al., *Biochemical and biophysical comparison of native and chemically synthesized phospholamban and a monomeric phospholamban analog.* J Biol Chem, 1996. **271**(3): p. 1669-77.
122. Mayer, E.J., G.M. Savage, and R.G. Johnson, Jr., *A quantitative immunoassay for the measurement of phospholamban levels and phosphorylation states. Measurement of phospholamban levels in transgenic mouse hearts.* Ann N Y Acad Sci, 1998. **853**: p. 284-7.
123. Colyer, J. and J.H. Wang, *Dependence of cardiac sarcoplasmic reticulum calcium pump activity on the phosphorylation status of phospholamban.* J Biol Chem, 1991. **266**(26): p. 17486-93.
124. Gallon, C.E., *Current techniques for the study of troponin I phosphorylation in human heart.* J Muscle Res Cell Motil, 2008. **29**(6-8): p. 169-72.
125. Dunn, J.D., G.E. Reid, and M.L. Bruening, *Techniques for phosphopeptide enrichment prior to analysis by mass spectrometry.* Mass Spectrom Rev. **29**(1): p. 29-54.
126. Olive, D.M., *Quantitative methods for the analysis of protein phosphorylation in drug development.* Expert Rev Proteomics, 2004. **1**(3): p. 327-41.
127. *The Immune system*. 2004 [cited 2012 10/27/12]; Available from: http://www.uic.edu/classes/bios/bios100/lecturesf04am/lect23.htm.
128. Levinson, W., *Medical Microbiology & Immunology*. 2004, New York: Lange Medical Books/McGraw Hill. 383-392.
129. Charles A Janeway, J., Paul Travers, Mark Walport, and Mark J Shlomchik, *The Immune System in Health and Disease*. 5th ed. Immunobiology. 2001, New York: Garland Publishing.
130. Kindt, T., Goldsby, RA, Osbourne, BA, *Kuby Immunology*. 6th ed. 2007, New York: W. H. Freeman and company.

131. Berg, J.M., Tymoczko, John L., Stryer, Lubert, *Biochemistry*. 5th ed. 2002, New York: W. H. Freeman and Company.
132. Rhoades, R., Pflanzer, RG, *Human Physiology*. 4th ed. 2002: Thompson Learning.
133. Lockwood, N.A., et al., *Structure and function of integral membrane protein domains resolved by peptide-amphiphiles: application to phospholamban.* Biopolymers, 2003. **69**(3): p. 283-92.
134. Ablorh, N.A., et al., *Insulin-dependent rescue from cardiogenic shock is not mediated by phospholamban phosphorylation.* Clin Toxicol (Phila), 2009. **47**(4): p. 296-302.
135. Levine, M.D. and E. Boyer, *Hyperinsulinemia-euglycemia therapy: a useful tool in treating calcium channel blocker poisoning.* Crit Care, 2006. **10**(4): p. 149.
136. Brubacher, J., *Goldfrank's Toxicologic Emergencies*. Eighth ed. B-Adrenergic Antagonists, ed. G. Flomenbaum NE, LR, Hoffman RS, Howland MA, Lewin NA, Nelson LS. 2006, New York: McGraw-Hill.
137. Holger, J.S., et al., *Insulin versus vasopressin and epinephrine to treat beta-blocker toxicity.* Clin Toxicol (Phila), 2007. **45**(4): p. 396-401.
138. Kline, J.A., E. Leonova, and R.M. Raymond, *Beneficial myocardial metabolic effects of insulin during verapamil toxicity in the anesthetized canine.* Crit Care Med, 1995. **23**(7): p. 1251-63.
139. Tune, J.D., R.T. Mallet, and H.F. Downey, *Insulin improves contractile function during moderate ischemia in canine left ventricle.* Am J Physiol, 1998. **274**(5 Pt 2): p. H1574-81.
140. Ranasinghe, A.M., et al., *Glucose-insulin-potassium and tri-iodothyronine individually improve hemodynamic performance and are associated with reduced troponin I release after on-pump coronary artery bypass grafting.* Circulation, 2006. **114**(1 Suppl): p. I245-50.
141. Hamdulay, S.S., A. Al-Khafaji, and H. Montgomery, *Glucose-insulin and potassium infusions in septic shock.* Chest, 2006. **129**(3): p. 800-4.
142. Clerk, L.H., et al., *The vasodilatory actions of insulin on resistance and terminal arterioles and their impact on muscle glucose uptake.* Diabetes Metab Res Rev, 2004. **20**(1): p. 3-12.
143. Sundell, J., et al., *Dose-dependent vasodilating effects of insulin on adenosine-stimulated myocardial blood flow*. Diabetes, 2002. **51**(4): p. 1125-30.
144. Shepherd, G. and W. Klein-Schwartz, *High-dose insulin therapy for calcium-channel blocker overdose.* Ann Pharmacother, 2005. **39**(5): p. 923-30.
145. MacLennan, D.H., *Ca2+ signalling and muscle disease.* Eur J Biochem, 2000. **267**(17): p. 5291-7.
146. Bechtel, L.K., D.M. Haverstick, and C.P. Holstege, *Verapamil toxicity dysregulates the phosphatidylinositol 3-kinase pathway.* Acad Emerg Med, 2008. **15**(4): p. 368-74.
147. Leblais, V., et al., *Phosphatidylinositol 3-kinase offsets cAMP-mediated positive inotropic effect via inhibiting Ca2+ influx in cardiomyocytes.* Circ Res, 2004. **95**(12): p. 1183-90.

148. MacLennan, D.H., and Kranias, E. G., *Phospholamban: a crucial regulator of cardiac contractility.* Nature Reviews, 2003. **4**: p. 666-678.
149. Nediani, C., et al., *Biochemical changes and their relationship with morphological and functional findings in pig heart subjected to lasting volume overload: a possible role of acylphosphatase in the regulation of sarcoplasmic reticulum calcium pump.* Basic Res Cardiol, 2002. **97**(6): p. 469-78.
150. Heerdt, P.M., et al., *Nitrosative stress and myocardial sarcoplasmic endoreticular calcium adenosine triphosphatase subtype 2a activity after lung resection in swine.* Anesthesiology, 2007. **107**(6): p. 954-62.
151. Laemmli, U.K., *Cleavage of structural proteins during the assembly of the head of bacteriophage T4.* Nature, 1970. **227**(259): p. 680-5.
152. Karim, C.B., et al., *Role of cysteine residues in structural stability and function of a transmembrane helix bundle.* J Biol Chem, 2001. **276**(42): p. 38814-9.
153. Towbin, H., T. Staehelin, and J. Gordon, *Electrophoretic transfer of proteins from polyacrylamide gels to nitrocellulose sheets: procedure and some applications.* Proceedings of the National Academy of Sciences of the United States of America, 1979. **76**(9): p. 4350-4354.
154. Mayer, E.J., et al., *Characterization and Quantitation of Phospholamban and Its Phosphorylation State Using Antibodies.* Biochemical and Biophysical Research Communications, 2000. **267**(1): p. 40-48.
155. Vittone, L., et al., *Mechanisms involved in the acidosis enhancement of the isoproterenol-induced phosphorylation of phospholamban in the intact heart.* J Biol Chem, 1998. **273**(16): p. 9804-11.
156. Rapundalo, S.T., R.J. Solaro, and E.G. Kranias, *Inotropic responses to isoproterenol and phosphodiesterase inhibitors in intact guinea pig hearts: comparison of cyclic AMP levels and phosphorylation of sarcoplasmic reticulum and myofibrillar proteins.* Circ Res, 1989. **64**(1): p. 104-11.
157. Brownsey, R.W., A.N. Boone, and M.F. Allard, *Actions of insulin on the mammalian heart: metabolism, pathology and biochemical mechanisms.* Cardiovasc Res, 1997. **34**(1): p. 3-24.
158. Kline, J.A., et al., *Insulin improves heart function and metabolism during non-ischemic cardiogenic shock in awake canines.* Cardiovasc Res, 1997. **34**(2): p. 289-298.
159. Chang, L., S.-H. Chiang, and A.R. Saltiel, *TC10alpha Is Required for Insulin-Stimulated Glucose Uptake in Adipocytes.* Endocrinology, 2007. **148**(1): p. 27-33.
160. Kuschel, M., et al., *Ser16 prevails over Thr17 phospholamban phosphorylation in the beta-adrenergic regulation of cardiac relaxation.* Am J Physiol, 1999. **276**(5 Pt 2): p. H1625-33.
161. Li, L., et al., *Phosphorylation of phospholamban and troponin I in beta -adrenergic-induced acceleration of cardiac relaxation.* Am J Physiol Heart Circ Physiol, 2000. **278**(3): p. H769-779.
162. Morisco, C., et al., *Akt mediates the cross-talk between beta-adrenergic and insulin receptors in neonatal cardiomyocytes.* Circ Res, 2005. **96**(2): p. 180-8.
163. Tada, M., et al., *Mechanism of the stimulation of Ca2+-dependent ATPase of cardiac sarcoplasmic reticulum by adenosine 3':5'-monophosphate-dependent*

protein kinase. Role of the 22,000-dalton protein. J Biol Chem, 1979. **254**(2): p. 319-26.

164. Tada, M. and T. Toyofuku, *SR Ca(2+)-ATPase/phospholamban in cardiomyocyte function.* J Card Fail, 1996. **2**(4 Suppl): p. S77-85.
165. Tada, M., et al., *Role of phospholamban (22,000-dalton protein) in cyclic AMP-mediated control of Ca2+-dependent ATPase of cardiac sarcoplasmic reticulum.* Adv Myocardiol, 1980. **1**: p. 161-71.
166. Tada, M., et al., *Transient state kinetic studies of Ca2+-dependent ATPase and calcium transport by cardiac sarcoplasmic reticulum. Effect of cyclic AMP-dependent protein kinase-catalyzed phosphorylation of phospholamban.* J Biol Chem, 1980. **255**(5): p. 1985-92.
167. Beuckelmann, D.J., M. Nabauer, and E. Erdmann, *Intracellular calcium handling in isolated ventricular myocytes from patients with terminal heart failure.* Circulation, 1992. **85**(3): p. 1046-55.
168. Schwinger, R.H., et al., *Reduced Ca(2+)-sensitivity of SERCA 2a in failing human myocardium due to reduced serin-16 phospholamban phosphorylation.* J Mol Cell Cardiol, 1999. **31**(3): p. 479-91.
169. Chien, K.R., J. Ross, Jr., and M. Hoshijima, *Calcium and heart failure: the cycle game.* Nat Med, 2003. **9**(5): p. 508-9.
170. Simmerman, H., et al., *Sequence analysis of phospholamban. Identification of phosphorylation sites and two major structural domains.* J. Biol. Chem., 1986. **261**(28): p. 13333-13341.
171. Simmerman, H.K. and L.R. Jones, *Phospholamban: protein structure, mechanism of action, and role in cardiac function.* Physiol Rev, 1998. **78**(4): p. 921-47.
172. Huang, B., et al., *Diminished Basal Phosphorylation Level of Phospholamban in the Postinfarction Remodeled Rat Ventricle : Role of {beta}-Adrenergic Pathway, Gi Protein, Phosphodiesterase, and Phosphatases.* Circ Res, 1999. **85**(9): p. 848-855.
173. Lockamy, E.L., et al., *Functional and physical competition between phospholamban and its mutants provides insight into the molecular mechanism of gene therapy for heart failure.* Biochem Biophys Res Commun, 2011. **408**(3): p. 388-92.
174. MacLennan, D.H., M. Asahi, and A.R. Tupling, *The regulation of SERCA-type pumps by phospholamban and sarcolipin.* Ann N Y Acad Sci, 2003. **986**: p. 472-80.
175. Kranias, E.G. and D.M. Bers, *Calcium and cardiomyopathies.* Subcell Biochem, 2007. **45**: p. 523-37.
176. Asahi, M., et al., *Cardiac-specific overexpression of sarcolipin inhibits sarco(endo)plasmic reticulum Ca2+ ATPase (SERCA2a) activity and impairs cardiac function in mice. 10.1073/pnas.0402596101.* Proceedings of the National Academy of Sciences of the United States of America, 2004. **101**(25): p. 9199-9204.

177. Huke, S. and M. Periasamy, *Phosphorylation-status of phospholamban and calsequestrin modifies their affinity towards commonly used antibodies.* J Mol Cell Cardiol, 2004. **37**(3): p. 795-9.
178. Huke, S. and D.M. Bers, *Temporal dissociation of frequency-dependent acceleration of relaxation and protein phosphorylation by CaMKII.* Journal of Molecular and Cellular Cardiology, 2007. **42**(3): p. 590-599.
179. Gorbe, A., et al., *Role of cGMP-PKG signaling in the protection of neonatal rat cardiac myocytes subjected to simulated ischemia/reoxygenation.* Basic Res Cardiol. **105**(5): p. 643-50.
180. Ferrington, D.A., et al., *Comparable levels of Ca-ATPase inhibition by phospholamban in slow-twitch skeletal and cardiac sarcoplasmic reticulum.* Biochemistry, 2002. **41**(44): p. 13289-96.
181. Li, M., et al., *Phosphorylation-induced structural change in phospholamban and its mutants, detected by intrinsic fluorescence.* Biochemistry, 1998. **37**(21): p. 7869-77.
182. Luo, W., et al., *Transgenic approaches to define the functional role of dual site phospholamban phosphorylation.* J Biol Chem, 1998. **273**(8): p. 4734-9.
183. Kaye, D.M., et al., *Percutaneous cardiac recirculation-mediated gene transfer of an inhibitory phospholamban peptide reverses advanced heart failure in large animals.* J Am Coll Cardiol, 2007. **50**(3): p. 253-60.
184. Cooper, L.T., et al., *The role of endomyocardial biopsy in the management of cardiovascular disease: a scientific statement from the American Heart Association, the American College of Cardiology, and the European Society of Cardiology. Endorsed by the Heart Failure Society of America and the Heart Failure Association of the European Society of Cardiology.* J Am Coll Cardiol, 2007. **50**(19): p. 1914-31.